European Journal of Chemistry

Check for updates

View Journal Online
View Article Online

Comparative study of 4-((4-aminophenyl)diazenyl)-2-((2-phenylhydrazono) methyl)phenol and *N*-(4-((4-hydroxy-3-((2-phenylhydrazono)methyl)phenyl) diazenyl)phenyl)acetamide - DFT method

Richard Rajkumar Siluvairaj [1], Vallal Perumal Govindasamy [2], Rajarajan Govindasamy [2], Periyanayagasamy Vanathu Chinnappan [1] and Thanikachalam Venugopal [2,*]

[1] *Department of Chemistry, St. Joseph's College of Arts and Science, Cuddalore-607001, Tamilnadu, India*
[2] *Department of Chemistry, Annamalai University, Annamalainagar-608002, Tamilnadu, India*

* *Corresponding author at: Department of Chemistry, Annamalai University, Annamalainagar-608002, Tamilnadu, India.*
e-mail: pvta1998@yahoo.co.in (T. Venugopal).

RESEARCH ARTICLE

10.5155/eurjchem.15.1.50-70.2498

Received: 31 October 2023
Received in revised form: 09 January 2024
Accepted: 06 February 2024
Published online: 31 March 2024
Printed: 31 March 2024

KEYWORDS

NBO
HOMO-LUMO
Solvent effect
UV-Vis studies
Dihedral angle
Dipole moment

ABSTRACT

Theoretical calculation of 4-((4-aminophenyl)diazenyl)-2-((2-phenylhydrazono)methyl) phenol (1) and *N*-(4-((4-hydroxy-3-((2-phenylhydrazono)methyl)phenyl)diazenyl)phenyl) acetamide (2) was studied by DFT/B3LYP/6-311+G(d,p) basis set. The calculated values of geometric structural parameters, Fourier transform infrared spectral data, highest occupied molecular orbital and lowest unoccupied molecular orbital, natural bond orbital, nucleus-independent chemical shifts, Fukui function, polarizability, hyperpolarizability, and UV data of compounds 1 and 2 clearly indicate that substitution of the amino group alters the physical properties of compound 2. The nucleus-independent chemical shift values of the amino-substituted phenyl ring reduces the aromatic character due to the lone pair electron on nitrogen involved in inductive and conjunction effects, as well as due to OH, NH_2 and OH, $NHCOCH_3$ in compounds 1 and 2, respectively. The effect of the solvent on different parameters was studied, and it was found that increasing the dielectric constant increased the parameter studied. The stability and planarity of the molecule's effects on dipole moment, energy, polarizability, and hyperpolarizability were studied extensively.

Cite this: *Eur. J. Chem.* **2024**, *15(1)*, 50-70 **Journal website**: www.eurjchem.com

1. Introduction

Zubrys and Siebenmann have synthesized condensation products of iso-nicotinylhydrazones, monohydroxyl benzaldehydes, and the corresponding aldehyde phenoxyacetic acid. Of 6-methoxy-2-formylphenoxyacetic acid, these are considered to have the most pronounced antituberculous exertion combined with low toxin [1]. Thermal recyclization of 3-methyl-4-acetyl(benzoyl)furoxans(3-methyl-4-acetyl(benzoyl) -2-oxides)phenylhydrazonesto oximes of 5-acetyl-4-phenyl (methyl)-1-oxide and base-convinced mononuclear heterocyclic rearrangement of below phenylhydrazones to 4-phenyl (methyl)-5-(1-nitroethyl) were prepared by Baryshnikova and Makhova [2]. Dimmock *et al.* were synthesized colorful acetylhydrazones, oxamoylhydrazones, and semicarbazones as seeker anticonvulsants with a view to examining the viability of an apparent list thesis [3]. The natural results revealed that, in general, the acetylhydrazones and semicarbazones showed good protection against storms, whereas the oxamoyl-hydrazones were significantly less active. Sevim Rollas *et al.* prepared a series of hydrazidehydrazones and 1,3,4-oxadiazolines of 4-fluorobenzoic acid hydrazide [4]. These compounds were tested for their antibacterial and antifungal conditioning against *Staphylococcus aureus*, *Escherichia coli*, *Pseudomonas aeruginosa*, and *Candida albicans*. Rosanna Maccari *et al.* [5] studied an *in vitro* antimycobacterial of isoniazid-related isonicotinoylhydrazones (ISNE), 2'-monosubstituted isonicotino-hydrazides and cyanoboranes. The most intriguing result is that some hydrazides and ISNEs were shown to be more effective antimycobacterial agents than maternal isoniazid in a model of tuberculosis-infected macrophages. A new series of imidazo-(1,2-*a*)-pyrazine-2-carboxylic acid arylidenehydrazides was prepared and characterized by infrared spectroscopy (IR), proton nuclear magnetic resonance (^{1}H NMR), and fast atom bombardment mass spectrometry (FAB-MS) spectral data. Three compounds were also estimated for anti-tuberculosis exertion against *Mycobacterium tuberculosis* H37Rv using the BACTEC460 radiometric system and BACTEC12B medium. The compound showed moderately good assets against mortal pathogenic microorganisms and is inactive against *Mycobacterium tuberculosis* H37Rv [6].

https://dx.doi.org/10.5155/eurjchem.15.1.50-70.2498

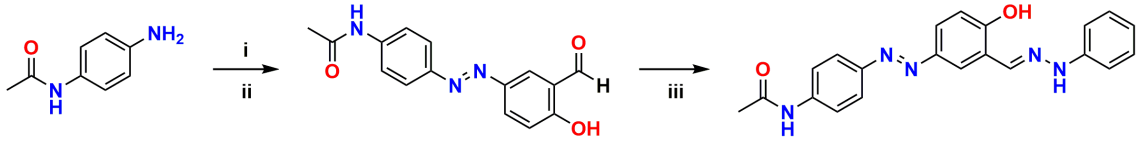

Scheme 1. Synthesis scheme for *N*-(4-((4-hydroxy-3-((2-phenylhydrazono)methyl)phenyl)diazenyl)phenyl)acetamide (**2**).

A series of 2-quinoxalinone-3-hydrazzone derivatives was prepared using a microwave oven system, structurally verified by logical and spectral data, and estimated for their antimicrobial conditioning. The mortal frame displayed pronounced energy as antimicrobial agents. The most active antibacterial agent was 3-{2-(1-(6-chloro-2-oxo-2*H*-chromen-3-yl)ethylidene) hydra-zinyl} quinoxalin-2(1*H*)-one, while (propanylidene)hydrazinyl) quinoxalin-2(1*H*)-one, appeared to be the most active antifungal agent [7].

The colorimetric and turn-off fluorescent selective detection of Cu^{2+} was attributed to the 2:1 complex of diarylethene and Cu^{2+} ions. In addition, the metal-responsive photochromic behavior of diarylethene was successfully applied to the construction of a molecular logic circuit [8]. A novel aryl hydrazone was synthesized *via* the Japp-Klingemann reaction between diazotized 4-aminoantipyrine and barbituric acid. Various spectroscopic methods and X-ray single-crystal analysis have characterized it. The effect of pH on the azo-hydra-zone tautomerism of the ligand has been studied with UV-vis spectroscopy. Two types of complexes were obtained by reaction of the ligand with copper sulphatepentahydrate in methanol under different experimental conditions [9]. In the case of polymorphism, different structures melt into the same liquid. The same structure melts in different liquids [10]. Sumita and Enoch reported the Mg^{2+} ion sensing behavior of the phenylhydrazone derivative of difluorenylpiperidin-4-one [11]. The composition and binding strength of the Mg^{2+} complex of phenylhydrazone are determined. The compound shows an association constant of 3375.36 M^{-1} for binding to Mg^{2+} ions. The detection range and competitive binding behavior of Mg^{2+} ions are reported. The phenylhydrazone of difluorenylpiperidin-4-one shows appreciable selectivity and detection sensitivity for Mg^{2+} ions. The molecular properties of 4-hydroxy-6-methyl-3-[(1*E*)-1-(2-phenylhydrazinylidene)ethyl]-2*H*-pyran-2-one (DHAA-PH) [12], have been carried out using the hybrid Density Functional Theory (DFT) and Time-Dependent Density Functional Theory (TDFT) methods at B3LYP/6-31+G(d,p) levels of theory. To substantiate the sensitivity of functionally applied M06-2X/6-311++G(2d,2p) and mPWB1W/6-311++G(2d,2p) were used to calculate geometric, IR, ^{1}H NMR, and energy gap calculations. DFT calculations with M06-2X and mPWB1W were predicted to agree with the experiment compared to B3LYP functional. Benzaldehydesemicarbazone (BSC) was grown by the slow evaporation technique for single crystals. The grown crystals were identified by the XRD method. The functional groups were identified from the FT-IR spectrum. UV-vis and thermal gravimetric analyses were performed [13]. The data of the literature show that no theoretical studies of the compounds 4-((4-aminophenyl)diazenyl)-2-((2-phenyl hydrazono)methyl) phenol (**1**) and *N*-(4-((4-hydroxy-3-((2-phenylhydrazono)-methyl)phenyl)-diazenyl)phenyl)acetamide (**2**) was studied using the DFT/B3LYP/6-311+G(d,p). Compound **1** is not synthesized and is used only for theoretical comparisons.

2. Experimental

2.1. Synthesis of N-(4-((4- hydroxy-3-((2-phenylhydrazono) methyl)phenyl)diazenyl)phenyl)acetamide (2)

A substituted imine derivative was synthesized as a two-step synthetic protocol. To the azo dye *N*-(4-((3-formyl-4-hydroxyphenyl)diazenyl)phenyl)acetamide (parent compound) (0.4 g) obtained, 0.5 g of phenylhydrazine hydrochloride and 0.8 g of sodium acetate were added and refluxed for 15 minutes in ethanol to obtain compound (*N*-(4-((4-hydroxy-3-((2-phenylhydrazono)methyl)phenyl)diazenyl)phenyl)acetamide) , from now referred to as compound **2**, which was recrystallized from ethanol [14]. Microanalysis, IR, ^{1}H, ^{13}C NMR, and UV spectra characterized the compound obtained. The synthesized compound **2** and its amine counterpart 4-((4-amino phenyl) diazenyl)-2-((2-phenylhydrazono)methyl)phenol from now on referred to as compound **1** were studied using the DFT method (Scheme 1).

N-(4-((4-Hydroxy-3-((2-phenyl hydrazono)methyl)phenyl) diazenyl)phenyl)acetamide (**2**): Color: Yellow. Yield: 78%. M.p.: 120-122 °C. FT-IR (KBr, ν, cm^{-1}): 3300 (OH), 1650 (C=O). ^{1}H NMR (400 MHz, DMSO-d_6, ppm): 11.12 (s, 1H, NH), 10.56 (s, 1H, NH), 10.29 (s, 1H, OH), 8.223-6.772 (m, 12H, ArH + 1H, CH=N), 2.098 (s, 3H, CH_3). ^{13}C NMR (100 MHz, DMSO-d_6, ppm): 169.17 (C-O), 158.53 (C=N), 148.00 (C-N), 145.90 (C-N), 145.18 (C-N), 142.20, 139.00, 137.00, 129.77, 129.77, 123.7, 119.60, 112.18 (Ar-C), 24.00 (C-H). Anal. calcd. for $C_{21}H_{19}N_5O_2$: C, 67.55; H, 5.13; N, 18.76. Found: C, 67.05; H, 5.08; N, 18.70%. UV/Vis ($CHCl_3$, λ_{max}, nm, (ε)): 355 (3.62).

2.2. Computational details

Geometry optimization and vibrational frequency calculations have been performed at DFT hybrid B3LYP/6-311+G(d,p) level theory. The general tendency of the quantum chemical method is to overestimate the force constant at the exact equilibrium geometry of the molecule [15]. Hence, the hybrid DFT hybrid B3LYP functional method was used for obtaining considerably better agreement with experimental data [16]. The molecular orbital (MO) figures were prepared using the GaussView 3.09 package [17] with a contour value of 0.020, and the molecular orbital contributions (MOCs) of different molecular parts were calculated at the B3LYP/6-311+G(d,p) level. A great variety of quantum chemical indices were taken from the calculation results, such as the energy of the highest occupied molecular orbital (HOMO), the energy of the lowest unoccupied molecular orbital (LUMO), electronegativity, global hardness and softness, electron affinity, ionization potential, *etc*. These quantities are often defined following the Koopmans' theorem [18]. Electronegativity (χ) is the measure of the power of an electron or a group of atoms to attract electrons toward itself [19], and according to the Koopmans' theorem, it was estimated using Equation 1, so the other global parameters were calculated using Equations 2-4.

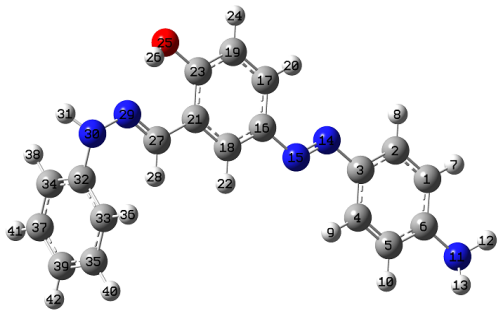

Figure 1. Optimized structure of compound **1**.

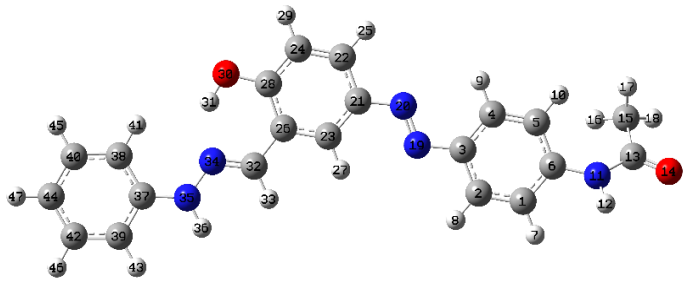

Figure 2. Optimized structure of compound **2**.

The Fukui function (FF) [20] is one of the most widely used local density functional descriptors to model chemical reactivity and site selectivity. It is defined as the derivative of the electron density ρ(r) with respect to the total number of electrons N in the system at a constant external potential V(r) acting on an electron due to all nuclei in the system, and therefore Mulliken population analyzes were performed on the optimized geometries of neutral, cationic and anionic states of the investigated molecules. Mulliken charges of each atom in neutral and charged states were substituted in the equations proposed by Yang and Mortier [21], based on a finite-difference method.

$$\chi = \frac{E_{HOMO}+E_{LUMO}}{2} \quad (1)$$

$$f_k^+ = q_k(N+1) - q_k\ (N) \text{ for nucleophilic attack} \quad (2)$$

$$f_k^- = q_k(N) - q_k\ (N\text{-}1) \text{ for electrophilic attack} \quad (3)$$

$$f_k^o = q_k(N+1) - q_k\ (N) \quad (4)$$

For a radical attack to evaluate the Fukui indices. Again, Fukui indices and global indices were substituted in Equations 5-9 to determine the local reactivity indices such as local philicity, local softness, relative nucleophilicity (S_k^-/S_k^+), relative electrophilicity (S_k^+/S_k^-), dual descriptor ($\Delta f(r)$), dual local softness ΔS_k, and multiphilic descriptor $\Delta\omega_k$.

$$\omega_k^\alpha = \omega f_k^\alpha \quad (5)$$

$$S_k^\alpha = S f_k^\alpha \quad (6)$$

$$\Delta f(r) = [(f^+(r) - (f^-(r)] \quad (7)$$

$$\Delta s_k = S\,(f_k^+ - f_k^-) = s_k^+ - s_k^- \quad (8)$$

$$\Delta\omega_k = [\omega_k^+ - \omega_k^-] = \omega\,[\Delta f_k] \quad (9)$$

where (α = +, -, and 0) represent local philic quantities that describe nucleophilic, electrophilic, and radical attacks, respectively. The condensed Fukui function, local softness, and multiphilic descriptor for each reactive atom of the candidate molecule was calculated using Mulliken population analysis [22]. Nuclear magnetic resonance (NMR)/nucleus-independent chemical shift (NICS) calculations [23,24] for all test molecules were performed using the gauge-including-atomic-orbital (GIAO) method with the basis set B3LYP/6-311+G(2d,p). NICS(1)zz was calculated using the component of the magnetic shift tensor in the z-direction, perpendicular to the plane of the ring, for a dummy atom 2 Å above [25], the plane of the ring. The NICS [23,24,26] probes (Bq) were placed up and down from the geometric center of the ring, perpendicular to the average ring plane, from -2 to +2 Å, in increments of 0.2 Å. The NICS values [23,24] were calculated for all ghost atoms using the Gaussian 09 software package [17]. The appropriate structural parameters of the optimized structure of the given molecule obtained using the B3LYP method with a 6-311+G(d,p) basis set have been used for the calculation of the Harmonic Oscillator Model of Aromaticity (HOMA) [24,27], values. The non-linear optical (NLO) properties were evaluated at the DFT level based. Based on the geometries of the ground state, where μ and α_{ij} have been calculated analytically [28]. β_{ijk} has been computed by using the afinite field procedure based on the numerical differentiation of the analytic polarizabilities evaluated under several electric field amplitudes. The first hyperpolarizability (β_0) and related properties (β, 0, and Δ) for the respective molecules (from the components of β) were calculated.

3. Results and discussion

3.1. Optimized parameters

The optimized parameters of compounds **1** and **2** are presented in Tables 1 and 2, and Figures 1 and 2, the C-C bond lengths of the phenyl ring vary between 1.3817-1.4159 Å for compound **1**, 1.3848-1.4246 Å for compound **2**. In the present study, the computed C-N bonds for compound **1** is from 1.3859 to 1.4365 Å and for compound **2** from 1.3862-1.4139 Å, and their XRD values are 1.3680-1.3776 Å [29,30].

Table 1. Geometric bond lengths (Å), bond angles, and dihedral angles (°) of compound **1** calculated with DFT-B3LYP/6-311+G(d,p) basis set.

Bond length, Å	B3LYP/6-311+G(d,p)	Bond angle, °	B3LYP/6-311+G(d,p)	Dihedral angle, °	B3LYP/6-311+G(d,p)
C1-C2	1.3866	N15-C16-C18	120.1	C1-C6-N11-H13	161.4
C1-C6	1.4043	C17-C16-C18	119.5	C5-C6-N11-H12	-162.0
C1-H7	1.0850	C16-C17-C19	120.2	C5-C6-N11-H13	-21.1
C2-C3	1.3985	C16-C17-H20	119.6	C3-C14-N15-C16	179.9
C2-H8	1.0839	C19-C17-H20	120.3	N14-N15-C16-C17	-91.6
C3-C4	1.4043	C16-C18-C21	121.3	N14-N15-C16-C18	93.0
C3-N14	1.4166	C16-C18-H22	119.4	N15-C16-C17-C19	-176.4
C4-C5	1.3817	C21-C18-H22	119.3	N15-C16-C17-H20	3.7
C4-H9	1.0827	C17-C19-C23	120.8	C18-C16-C17-C19	-0.9
C5-C6	1.4107	C17-C19-H24	121.0	C18-C16-C17-H20	179.2
C5-H10	1.0856	C23-C19-H24	118.3	N15-C16-C18-C21	176.5
C6-N11	1.3856	C18-C21-C23	118.7	N15-C16-C18-H22	-3.7
N11-H12	1.0082	C18-C21-C27	118.7	C17-C16-C18-C21	1.0
N11-H13	1.0082	C23-C21-C27	122.6	C17-C16-C18-H22	-179.2
N14-N15	1.2487	C19-C23-C21	119.5	C16-C17-C19-C23	0.3
N15-C16	1.4365	C19-C23-O25	118.2	C16-C17-C19-H24	-179.5
C16-C17	1.3978	C21-C23-O25	122.2	H20-C17-C19-C23	-179.8
C16-C18	1.3861	C23-O25-H26	107.8	H20-C17-C19-H24	0.3
C17-C19	1.3886	C21-C27-H28	116.7	C16-C18-C21-C23	-0.5
C17-H20	1.0838	C21-C27-N29	121.3	C16-C18-C21-C27	179.6
C18-C21	1.4060	H28-C27-N29	122.0	H22-C18-C21-C23	179.7
C18-H22	1.0850	C27-N29-N30	122.4	H22-C18-C21-C27	-0.2
C19-C23	1.3968	N29-N30-H31	108.9	C17-C19-C23-C21	0.2
C19-H24	1.0835	N29-N30-C32	124.7	C17-C19-C23-O25	-180.0
C21-C23	1.4159	H31-N30-C32	114.4	H24-C19-C23-C21	-180.0
C21-C27	1.4579	N30-C32-C33	120.5	H24-C19-C23-O25	-0.2
C23-O25	1.3523	N30-C32-C34	120.0	C18-C21-C23-C19	-0.1
O25-H26	0.9828	C33-C32-C34	119.4	C18-C21-C23-O25	-179.9
C27-H28	1.0898	C32-C33-C35	120.0	C27-C21-C23-C19	179.8
C27-N29	1.2878	C32-C33-H36	119.6	C27-C21-C23-O25	0.0
N29-N30	1.3789	C35-C33-H36	120.4	C18-C21-C27-H28	0.9
N30-H31	1.0094	C32-C34-C37	120.3	C18-C21-C27-N29	-178.8
N30-C32	1.4222	C32-C34-H38	119.5	C23-C21-C27-H28	-179.0
C32-C33	1.4005	C37-C34-H38	120.2	C23-C21-C27-N29	1.3
C32-C34	1.3988	C33-C35-C39	120.5	C19-C23-O25-H26	-179.7
C33-C35	1.3916	C33-C35-H40	119.5	C21-C23-O25-H26	0.1
C33-H36	1.0834	C39-C35-H40	120.0	C21-C27-N29-N30	-177.9
C34-C37	1.3934	C34-C37-C39	120.2	H28-C27-N29-N30	2.5
C34-C38	1.0851	C34-C37-H41	119.6	C27-N29-N30-H31	-155.3
C35-C39	1.3953	C39-C37-H41	120.2	C27-N29-N30-C32	-15.2
C35-H40	1.0842	C35-C39-C37	119.6	N29-N30-C32-C33	69.7
C37-C39	1.3931	C35-C39-H42	120.2	N29-N30-C32-C34	-113.8
C37-H41	1.0842	C37-C39-H42	120.2	H31-N30-C32-C33	-152.0
C39-H42	1.0837			H31-N30-C32-C34	24.4
Bond angle, °	**B3LYP/6-311+G(d,p)**	**Dihedral angle, °**	**B3LYP/6-311+G(d,p)**	**Dihedral angle, °**	**B3LYP/6-311+G(d,p)**
C2-C1-C6	120.2	H7-C1-C2-C8	-0.3	N30-C32-C33-C35	177.5
C2-C1-H7	120.1	C2-C1-C6-C5	0.1	N30-C32-C33-H36	-0.8
C6-C1-H7	119.7	C2-C1-C6-N11	177.7	C34-C32-C33-C35	1.0
C1-C2-C3	120.9	H7-C1-C6-C5	-179.7	C34-C32-C33-H36	-177.2
C1-C2-H8	120.8	H7-C1-C6-N11	-2.2	N30-C32-C34-C37	-176.2
C3-C2-H8	118.4	C1-C2-C3-C4	0.1	N30-C32-C34-H38	3.9
C2-C3-C4	119.1	C1-C2-C3-N14	-179.9	C33-C32-C34-C37	0.3
C2-C3-N14	115.9	H8-C2-C3-C4	-179.9	C33-C32-C34-H38	-179.6
C4-C3-N14	125.0	H8-C2-C3-N14	0.1	C32-C33-C35-C39	-1.3
C3-C4-C5	120.2	C2-C3-C4-C5	-0.1	C32-C33-C35-H40	180.0
C3-C4-H9	119.0	C2-C3-C4-H9	179.9	H36-C33-C35-39	176.9
C5-C4-H9	120.7	N14-C3-C4-C5	-180.0	H36-C33-C35-H40	-1.8
C4-C5-C6	120.8	N14-C3-C4-H9	-0.1	C32-C34-C37-C39	-1.3
C4-C5-H10	119.9	C2-C3-N14-N15	179.0	C32-C34-C37-H41	179.5
C6-C5-H10	119.3	C4-C3-N14-N15	-1.1	H38-C34-C37-39	178.6
C1-C6-C5	118.7	C3-C4-C5-C6	0.0	H38-C34-C37-H41	-0.6
C1-C6-N11	120.9	C3-C4-C5-H10	-179.8	C33-C35-C39-C37	0.3
C5-C6-N11	120.4	H9-C4-C5-C6	-179.9	C33-C35-C39-H42	-179.4
C6-C11-H12	117.3	H9-C4-C5-H10	0.3	H40-C35-C39-C37	179.0
C6-N11-H13	117.3	C4-C5-C6-C1	-0.1	H40-C35-C39-H42	-0.7
C12-N11-H13	113.8	C4-C5-C6-N11	-177.6	C34-C37-C39-C35	1.0
C3-N14-N15	115.9	H10-C5-C6-C1	179.7	C34-C37-C39-H42	-179.4
N14-N15-C16	113.8	H10-C5-C6-N11	2.2	H41-C37-C39-C35	-179.8
N15-C16-C17	120.2	C1-C6-N11-H12	20.5	H41-C37-C39-H42	-0.1

The optimized N-H bond distance ranges from 1.0082 to 1.0094 Å in compound **1**, 1.0125-1.0144 Å in compound **2** are comparable to the literature value of 0.85 Å [31]. The optimized C-H bond lengths vary from 1.0809-1.0858 Å for compounds **1** and **2**. The theoretical bond angles of C-C-C, C-C-H and C-N-N, C-N-H, C-N-N, N-N-C and N-N-H range from 115.9-120.4° [32]. The theoretical dihedral angles of the title molecules are given in Tables 1 and 2. Compound **1** is not synthesized and is used only for theoretical comparisons.

3.2. Vibrational assignments

Vibrational spectroscopy is widely employed in organic chemistry for the identification of functional groups, to study molecular conformations, reactions, *etc*. The resulting vibrational wave numbers for the optimized geometry of compounds **1** and **2** and the proposed assignments are given in Tables 3 and 4.

Table 2. Geometric bond lengths (Å), bond angles, and dihedral angles (°) of compound **2** calculated with DFT-B3LYP/6-311+G(d,p) basis set.

Bond length, Å	B3LYP/6-311+G(d,p)	Bond angle, °	B3LYP/6-311+G(d,p)	Dihedral angle, °	B3LYP/6-311+G(d,p)
C1-C2	1.3876	H16-C15-H17	108.4	C1-C6-N11-C13	140.4
C1-C6	1.4012	H16-C15-H18	110.2	C5-C6-N11-H12	145.1
C1-H7	1.0846	H17-C15-H18	107.8	C5-C6-N11-C13	-42.6
C2-C3	1.3994	C3-N19-N20	115.3	C6-N11-C13-O14	-179.8
C2-H8	1.0836	N19-N20-C21	115.8	C6-N11-C13-C15	-1.0
C3-C4	1.4033	N20-C21-C22	1160	H12-N11-C13-O14	-7.2
C3-N19	1.4139	N20-C21-C23	124.8	H12-N11-C13-C15	171.6
C4-C5	1.3857	C22-C21-C23	119.1	N11-C13-C15-H16	-31.1
C4-H9	1.0821	C21-C22-C24	120.7	N11-C13-C15-H17	90.2
C5-C6	1.4046	C21-C22-H25	118.4	N11-C13-C15-H18	-152.8
C5-H10	1.0819	C24-C22-H25	120.8	O14-C13-C15-H16	147.7
C6-N11	1.4109	C21-C23-C26	121.3	O14-C13-C15-H17	-91.0
N11-H12	1.0125	C21-C23-H27	118.7	O14-C13-C15-H18	26.0
N11-C13	1.3862	C26-C23-H27	120.0	C3-N19-N20-C21	-179.9
C13-O14	1.2188	C22-C24-C28	120.3	N19-N20-C21-C22	179.7
C13-C15	1.5137	C22-C24-H29	121.4	N19-N20-C21-C23	-0.3
C15-H16	1.0903	C28-C24-H29	118.3	N20-C21-C22-C24	-180.0
C15-H17	1.0935	C23-C26-C28	118.7	N20-C21-C22-H25	0.0
C15-H18	1.0890	C23-C26-C32	119.1	C23-C21-C22-C24	0.0
N19-N20	1.2561	C28-C26-C32	122.2	C23-C21-C22-H25	-180.0
N20-C21	1.4100	C24-C28-C26	119.9	N20-C21-C23-C26	-179.9
C21-C22	1.4035	C24-C28-O30	118.2	N20-C21-C23-H27	0.0
C21-C23	1.3979	C26-C28-O30	121.9	C22-C21-C23-C26	0.0
C22-C24	1.3848	C28-O30-H31	108.2	C22-C21-C23-H27	180.0
C22-H25	1.0835	C26-C32-H33	116.9	C21-C22-C24-C28	-0.1
C23-C26	1.3970	C26-H32-N34	122.5	C21-C22-C24-H29	179.9
C23-H27	1.0834	H33-C32-N34	120.6	H25-C22-C24-C28	179.9
C24-C28	1.3975	C32-N34-N35	119.1	H25-C22-C24-H29	0.0
C24-H29	1.0830	N34-N35-H36	118.5	C21-C23-C26-C28	-0.1
C26-C28	1.4246	N34-N35-C37	123.2	C21-C23-C26-C32	179.9
C26-C32	1.4540	H36-N35-C37	118.2	H27-C23-C26-C28	180.0
C28-O30	1.3446	N35-C37-C38	122.5	H27-C23-C26-C32	0.0
O30-H31	0.9819	N35-C37-C39	118.1	C22-C24-C28-C26	0.1
C32-H33	1.0951	C38-C37-C39	119.4	C22-C24-C28-O30	-180.0
C32-N34	1.2913	C37-C38-C40	119.6	H29-C24-C28-C26	-180.0
N34-N35	1.3437	C37-C38-H41	120.3	H29-C24-C28-O30	0.0
N35-H36	1.0144	C40-C38-H41	120.1	C23-C26-C28-C24	0.0
N35-C37	1.3954	C37-C39-C42	120.2	C23-C26-C28-O30	-180.0
C37-C38	1.4005	C37-C39-H43	119.8	C32-C26-C28-C24	-180.0
C37-C39	1.4033	C42-C39-H43	120.0	C32-C26-C28-O30	0.0
C38-C40	1.3921	C38-C40-C44	121.2	C23-C26-C32-H33	0.5
C38-H41	1.0809	C38-C40-H45	118.9	C23-C26-C32-N34	-179.5
C39-C42	1.3894	C44-C40-H45	120.0	C28-C26-C32-H33	-179.5
C39-H43	1.0858	C39-C42-C44	120.6	C28-C26-C32-N34	0.5
C40-C44	1.3937	C39-C42-H46	119.3	C24-C28-O30-H31	180.0
C40-H45	1.0843	C44-C42-H46	120.2	C26-C28-O30-H31	0.0
C42-C44	1.3949	C40-C44-C42	119.0	C26-C32-N34-N35	-179.6
C42-H46	1.0842	C40-C44-H47	120.5	H33-C32-N34-N35	0.4
C44-H47	1.0832	C42-C44-H47	120.5	C32-N34-N35-H36	-0.7
Bond angle, °	**B3LYP/6-311+G(d,p)**	**Dihedral angles, °**	**B3LYP/6-311+G(d,p)**	**Dihedral angles, °**	**B3LYP/6-311+G(d,p)**
C2-C1-C6	120.4	C6-C1-C2-C3	0.7	C32-N34-N35-C37	-178.1
C2-C1-H7	120.1	C6-C1-C2-H8	179.9	N34-N35-C37-C38	-0.4
C6-C1-H7	119.5	H7-C1-C2-C3	-178.7	N34-N35-C37-C39	179.7
C1-C2-C3	120.6	H7-C1-C2-H8	0.5	H36-N35-C37-C38	-177.8
C1-C2-H8	120.8	C2-C1-C6-C5	0.8	H36-N35-C37-C39	2.3
C3-C2-H8	118.6	C2-C1-C6-N11	177.9	N35-C37-C38-C40	-179.8
C2-C3-C4	119.0	H7-C1-C6-C5	-179.8	N35-C37-C38-H41	0.3
C2-C3-N19	116.0	H7-C1-C6-N11	-2.7	C39-C37-C38-C40	0.1
C4-C3-N19	125.0	C1-C2-C3-C4	-1.2	C39-C37-C38-H41	-179.8
C3-C4-C5	120.4	C1-C2-C3-N19	179.5	N35-C37-C39-C42	179.9
C3-C4-H9	119.0	H8-C2-C3-C4	179.6	N35-C37-C39-H43	-0.1
C5-C4-H9	120.6	H8-C2-C3-N19	0.3	C38-C37-C39-C42	0.0
C4-C5-C6	120.6	C2-C3-C4-C5	0.2	C38-C37-C39-H43	-180.0
C4-C5-H10	119.5	C2-C3-C4-H9	-178.3	C37-C38-C40-C44	0.0
C6-C5-H10	119.9	N19-C3-C4-C5	179.4	C37-C38-C40-H45	-180.0
C1-C6-C5	118.9	N19-C3-C4-H9	0.9	H41-C38-C40-C44	179.8
C1-C6-N11	118.5	C2-C3-N19-N20	-179.1	H41-C38-C40-H45	-0.1
C5-C6-N11	122.5	C4-C3-N19-N20	1.6	C37-C39-C42-C44	0.0
C6-N11-H12	116.3	C3-C4-C5-C6	1.3	C37-C39-C42-H46	180.0
C6-N11-C13	131.8	C3-C4-C5-H10	-176.9	H43-C39-C42-C44	179.9
H12-N11-C13	111.5	H9-C4-C5-C6	179.8	H43-C39-C42-H46	-0.1
N11-C13-O14	119.1	H9-C4-C5-H10	1.6	C38-C40-C44-C42	0.0
N11-C13-C15	119.0	C4-C5-C6-C1	-1.8	C38-C40-C44-H47	-180.0
O14-C13-C15	121.8	C4-C5-C6-N11	-178.8	H45-C40-C44-C42	179.9
C13-C15-H16	113.2	H10-C5-C6-C1	176.4	H45-C40-C44-H47	-0.1
C13-C15-H17	109.9	H10-C5-C6-N11	-0.5	C39-C42-C44-C40	0.0
C13-C15-H18	107.3	C1-C6-N11-C12	-31.9	C39-C42-C44-H47	-180.0

Table 3. Vibrational wavenumbers obtained for compound **1** with DFT-B3LYP/6-311+G(d,p) (Harmonic frequency (cm^{-1}), IR intensity, Raman activity (Km/mol), reduced masses (a.m.u.) and force constants (N/m)) *.

Mode no	Calculated freq. (cm^{-1})	IR intensity	Raman activity	Reduced mass	Force constant	Vibrational assignments with >10% PED
1	3543	23.40	86.76	1.10	8.82	νN11-H12+N11-H13(50)
2	3462	34.20	298.58	1.08	8.23	νN30-H31(100)
3	3444	72.92	537.60	1.05	7.92	νN11-H12+N11-H13(50)
4	3279	383.25	95.10	1.07	7.32	νO25-H26(99)
5	3078	2.13	58.00	1.09	6.60	νC4-H9(97)
6	3066	9.68	209.34	1.09	6.58	νC17-H20(32)+C10-H24(67)+C35-H40(26)+C37-H41(11)+C39-42(32)
7	3064	4.96	101.33	1.09	6.56	νC2-H8(91)
8	3055	17.01	53.49	1.09	6.55	νC33-H36(50)+C37-H41(21)+C39-H42(23)
9	3046	13.45	110.29	1.09	6.50	νC17-H20(68)+C19-H24(32)+C33-H36(11)+C34-H38(17)+C35-40(18)+C437-H41(38)+ C39-H42(14)
10	3045	0.35	89.00	1.09	6.44	νC33-H36(10)+C34-H38(18)+C35-H40(18)+C39-H42(23)
11	3040	3.91	23.91	1.09	6.45	νC18-H22(98)
12	3039	18.57	123.82	1.09	6.42	νC1-H7(91)
13	3033	5.48	35.99	1.09	6.40	νC34-H38(60)+C37-H41(28)
14	3156	21.66	142.02	1.09	6.39	νC5-H10(97)
15	1602	27.99	774.98	4.74	7.75	νN29-C27(51)
16	1601	266.42	90.85	1.54	2.52	βH13-C39-C37(61)
17	1590	6.15	1163.86	5.49	8.86	νC16-C18(10)+C23-C19(22)+C18-C21(17)
18	1585	29.07	55.61	2.74	4.38	νNC5-C4(19)+C2-C3(10)+βH13-N11-H12(23)
19	1582	27.07	45.61	4.75	4.38	νC39-C37(19)+C35-C39(22)+βC33-C35-C39(12)+H40-C35-C39(10)
20	1573	44.65	128.07	5.40	8.53	νC33-C35(28)+C39-C37(18)+βC32-C34-C35(10)
21	1564	19.30	14.88	5.00	7.80	νC32-C34(27)+C39-C39(15)+C32-C34(27)
22	1552	12.89	342.54	4.52	6.96	νC17-C16(17)
23	1549	13.03	205.62	5.68	8.70	νC2-C3(19)+C6-C1(20)
24	1505	379.59	2157.63	6.99	10.09	νN14-N15(19)
25	1471	25.50	27.69	1.58	2.18	βH31-N30-N29(45)
26	1467	5.22	932.58	2.75	3.78	νN14-N15(10)+βH9-C4-C5(18)+νN14-N15(100029
27	1453	210.40	235.06	2.83	3.81	βH20-C4-C19(10)+H22-C18-C21(16)+H24-C19-C23(25)
28	1423	6.71	91.74	2.28	2.97	νC16-C18(10)+βH26-O25-C23(22)
29	1409	41.24	215.10	3.25	4.14	νNC5-C4(17)+νC1-C2(24)+βH7-C1-C2(13)+H10-H10-C5-C6(13)+νNC1-C2(24)
30	1403	11.59	209.93	1.81	2.29	βH26-O25-C23(19)+H31-N30-N29(11)+H42-C39-C37(11)
31	1359	89.15	11.14	2.21	2.62	νC19-C17(15)+C18-C21(18)+βH26-O25-C23(18)
32	1312	16.89	7.29	1.65	1.84	βH28-C27-N29(39)
33	1307	0.23	11.22	5.19	5.69	νC4-C3(16)+C6-C1(24)C++C5-C4(17)+βH22-N11-C6(11)
34	1292	0.18	15.99	1.97	2.12	νC33-C35(14)+C34-C37(14)+βH36-C33-C25(19)+H38-C34-C37(21)+H42-C39-C37(11)
35	1281	3.99	427.97	3.81	4.02	νC16-C18(27)+C19-C17(12)
36	1274	4.69	13.25	1.60	1.67	βH7-C1-C2(12)+H8-C2-C1(18)+H9-C4-C5(18)+H10-C5-C6(17)
37	1259	145.63	68.30	3.18	3.23	νNC1-C2(11)+N11-C6(44)
38	1257	48.23	6.76	2.70	2.73	νC32-C34(25)+C35-C39(11)
39	1242	221.10	8.36	2.78	2.75	νO25-C23(16)βH20-C17-C19(21)
40	1215	14.85	203.37	2.56	2.42	νC18-C21(23)+N15-C16(10)+βH22-C18-C21(15)
41	1196	97.47	176.07	3.15	2.89	νN30-C32(36)
42	1192	74.82	121.23	2.27	2.07	νC23-C19(12)+N14-C3(12)+N15-C16(10)+βH22-C18-C21(13)
43	1175	71.70	458.02	2.41	2.13	νC23-C19(15)+C21-C27(10)+N30-C32(14)
44	1146	6.95	29.18	1.14	0.96	βH36-C33-C35(22)+H38-C34-C37(22)+H40-C35-C38(16)+H41-C37-C39(17)
45	1132	0.39	6.35	1.11	0.92	βH40-C35-C39(19)+H41-C37-C39(19)+H42-C39-C37(38)
46	1126	67.72	40.62	1.52	1.24	νN15-C16(12)+βH9-C4-C5(12)+H22-C18-C32(14)
47	1108	222.63	655.51	1.76	1.39	βH8-C2-C1(21)+νN14-C3(12)
48	1096	20.91	32.26	1.21	0.93	νC5-C4(10)+C1-C2(12)+βH7-C1-C2(15)+H9-C4-C5(17)
49	1093	7.77	2.95	1.42	1.09	νC16-C18(10)+C19-C17(12)+βH20-C17-C19(10)
50	1063	29.67	2.08	1.93	1.40	νC33-C35(11)+N29-N30(22)+βH38-C34-C37(14)
51	1041	33.81	2.02	2.77	1.93	νC34-C37(13)+N29-N30(35)
52	1025	3.46	2.12	1.42	0.96	νC6-C1(16)+βH12-N11-C6(50)
53	976	1.05	0.36	2.57	1.57	βC5-C4-C3(40)+C1-C2-C3(24)
54	972	0.11	84.26	6.06	3.68	νC35-C39(11)+βC33-C35-C39(29)+C34-C37-C39(15)+C35-C39-C37(19)
55	961	0.32	0.68	1.29	0.77	τH40-C35-C39-C37(26)+C41-C37-C39-C35(14)+C42-C39-C37-C34(31)+ C35-C39-C37-C34(10)
56	947	23.77	16.74	3.00	1.73	βC19-C17-C16(10)
57	945	0.22	0.61	1.34	0.77	τH9-C4-C1-C6(44)+H16-C5-C6-N11(19)+C5-C4-C3-C2(13)
58	943	3.30	0.15	1.46	0.83	τH36-C33-C35-C39(18)+H38-C34-C37-C39(11)+C40-C35-C39-C37(10)+ C41-C37-C39-C35(31)
59	927	1.29	0.24	1.34	0.74	τH7-C1-C2-C3(14)+H8-C2-C1-C6(50)+C6-C1-C2-C3(18)
60	920	7.38	1.93	1.46	0.79	τH20-C17-C19-C23(17)+H24-C19-C23-C21(16)+H28-C27-N29-30(45)+ τH28-C27-N29-N30(45)+H23-C17-C19-C23(17)+H24-C19-C23-C21(16)
61	914	4.59	3.94	1.49	0.80	τH20-C17-C19-C23(20)+H24-C19-C23-C21(16)+H28-C27-N29-N30(29)+ C23-C19-C17-C16(12)
62	896	6.58	9.26	2.68	1.38	βN14-N15-C16(10)
63	886	4.91	5.98	1.91	0.96	τH36-C33-C35-C39(17)+C38-C34-C37-C39(17)+C42-C39-C37-C34(17)
64	839	3.79	10.69	1.83	0.83	τH22-C18-C21-C23(36)
65	833	12.05	13.07	2.66	1.19	τH22-C18-C21-C23(15)
66	813	16.01	8.48	1.72	0.73	τH10-C5-C6-N11(10)+H36-C33-C35-C39(10)+H38-C34-C37-C39(13)
67	812	29.42	3.36	1.54	0.65	τH7-C1-C2-C3(16)+H10-C5-C6-N11(23)+H38-C34-C37-C39(14)
68	797	28.75	28.18	2.09	0.85	τH20-C17-C19-C23(26)+H24-C19-C23-C21(16)
69	774	0.58	0.11	1.26	0.50	τH7-C1-C2-C3(36)+H8-C2-C1-C6(17)+H9-C4-C5-C6(15)+H10-C5-C6-N11(29)
70	756	26.12	34.34	4.81	1.85	βC35-C39-C37(16)
71	739	17.27	19.79	4.82	1.77	βN15-C16-C18(13)+νO25-C23(16)
72	719	22.63	2.74	2.26	0.79	τC40-C35-C39-C37(10)+C41-C37-C39-C35(12)+C42-C39-C37-C34(13)+ C32-C34-C37-C39(12)+γN30-C33-C34-C32(13)
73	707	97.05	0.96	1.13	0.38	τH26-O25-C23-C19(82)

Table 3. (continued).

Mode no	Calculated freq. (cm^{-1})	IR intensity	Raman activity	Reduced mass	Force constant	Vibrational assignments with >10% PED
74	705	0.38	2.80	3.38	1.09	τH22-C18-C21-C23(13)+H24-C19-C25-C21(14)+O25-C19-C21-C23(18)
75	705	1.31	0.96	3.91	1.25	τC5-C4-C3-C2(17)+C6-C1-C2-C3(12)+γ N11-C5-C1-C6(22)
76	692	73.54	2.28	2.32	0.71	βC19-C17-C16(13)+τH42-C39-C37-C34(10)
77	627	2.33	13.42	6.30	1.59	βC6-C1-C2(17)+C5-C4-C3(15)+C1-C2-C3(24)
78	605	0.70	4.41	6.19	1.46	βC33-C35-C39(21)+C34-C37-C39(36)+C32-C34-C37(20)
79	578	6.42	4.13	4.68	1.00	βC3-N14-N15(19)
80	534	122.62	36.08	2.15	0.39	τH31-N30-N29-C27(23)+γ N11-C5-C1-C6
81	526	43.06	54.00	2.04	0.36	τH31-N30-N29-C27(28)+γ N11-C5-C1-C6(11)
82	488	8.82	3.01	3.66	0.56	βC32-C34-C37(10)+γN30-C33-C34-C32
83	486	16.81	7.74	4.35	0.66	βO25-C23-C19(19)+γN11-C5-C1-C6(12)
84	463	47.75	3.61	3.48	0.48	βC6-C1-C2(11)τH12-N11-C6-C5(12)+H13-N11-C6-C5(11)
85	459	25.92	4.47	3.51	0.47	βN14-N15-C16(11)+τC23-C19-C17-C16(10)
86	450	141.34	17.98	2.76	0.36	γ O25-C19-C21-C23(10)
87	449	59.46	12.10	3.76	0.49	τN15-C16-C18-C21(13)+γ O25-C19-C21-C23(18)
88	433	238.12	47.57	2.40	0.29	τH12-N11-C6-C5(42)+H13-N11-C6-C5(16)
89	415	3.82	1.00	3.42	0.38	βO25-C23-C19(13)+τC1-C2-C3-N14(13)+C6-C1-C2-C3(18)
90	399	2.20	2.55	4.24	0.43	βO25-C23-C19(25)+τC5-C4-C3-C2(14)
91	378	10.53	18.02	4.38	0.40	βC18-C21-C27(14)+N30+C32-C34(12)
92	374	11.25	5.22	3.54	0.32	βC6-C1-C2(11)+N11-C6-C1(39)
93	354	3.76	12.87	4.75	0.38	βN30-C32-C34(14)
94	334	12.80	0.73	1.12	0.08	τH12-N11-C6-C5(42)+H13-N11-C6-C5(42)
95	320	1.99	0.36	3.70	0.24	βN11-C6-C1(13)+τC16-C18-C21-C27(12)+C33-C19-C17-C16(12)
96	291	0.96	2.64	5.86	0.32	τC1-C2-C3-N14(10)+γ C4-C2-N14-C3(23)
97	269	2.21	2.45	5.01	0.23	τC16-C18-C21-C27(12)+C21-C27-N29-N30(19)+N15-C16-C18-C21(12)
98	241	2.52	1.97	3.91	0.15	βN30-C35-C34(15)+τC27-N29-N30-C32(17)+C18-C21-C27-N29(21)
99	178	0.79	6.03	6.03	0.12	βN14-N15-C16(11)+τC19-C17-C16-C18(10)
100	166	2.13	1.26	5.67	0.10	τC5-C4-C3-C2(11)+C1-C2-C3-N14(14)+C6-C1-C2-C3(13)
101	135	2.13	3.26	6.11	0.07	βC3-N14-N15(22)+τC19-C17-C16-C18(23)+N15-C16-C18-C21(15)
102	129	0.55	1.08	5.54	0.06	βC18-C21-C27(15)
103	119	0.06	6.15	7.55	0.07	τN14-N15-C16-C18(62)+C2-C3-N14-N15(16)
104	87	1.16	8.75	5.52	0.03	τC16-C18-C21-C27(26)+C18-C21-C27-N29(19)+C21-C27-N29-N30(15)
105	59	2.29	4.71	5.05	0.01	βC27-N29-N30(16)+C21-C27-N29(11)+τN29-N30-C32-C33(23)
106	51	0.15	2.96	5.74	0.01	βN14-N15-N16(14)+τC2-C3-N14-N15(19)+γC17-C18-N15-C16(18)

* ν: Stretching, β: In-plane bending, γ: Out-of-plane bending, ω: Wagging, t: Twisting, δ: Scissoring, ρ: Rocking.

The vibrational spectral data obtained from the solid-phase FT-IR spectra are assigned on the basis of the results of the normal coordinate calculations using the VEDA program to the computed vibrational frequencies in the Gaussian suite. On the basis of the comparison between the calculated and experimental results, assignments of fundamental modes were carried out. The assignment of the experimental frequencies is based on the observed band frequencies in the infrared spectra of this species, confirmed by establishing a one-to-one correlation between the observed and theoretically calculated frequencies. The calculated frequencies are slightly higher than the observed values for the majority of normal modes. Two factors may be responsible for the discrepancies between the experimental and computed spectra of azodye **2**. The first is caused by environmental conditions, and the second is due to the fact that the experimental value is an anharmonic frequency while the calculated value is a harmonic frequency [33]. The phenyl ring modes mostly involve C-C, and the vibrational frequency is associated with C-C stretching modes of the carbon skeleton. The C-C stretching modes predicted in the range 1600-1550 cm^{-1} are in agreement with the experimental observation of the IR value and the amine counterpart 1. The aromatic C-H stretching frequencies are found at 3090-3029 cm^{-1} (theoretical) for compound **2** (containing anilide moiety) coinciding with the experimental value of 3054 cm^{-1}, and the same trend is also observed in compound **1** (3156-3033 cm^{-1}) molecule as well. The stretching of CH between 3024-2992 cm^{-1} is due to the aliphatic group in compound **2**, and a similar stretching is missing in compound **1** molecule. The C13=O14 stretching at 1677 cm^{-1} matches the experimental value at 1650 cm^{-1}. N35-H36 is observed at 3387 cm^{-1}, its experimental observation is around 3307 cm^{-1}, and it is supported by a total energy distribution (TED) value of 99%, which is found at around 3462 cm^{-1} for N30-H31. The N-H stretching at 3543 cm^{-1} with a TED value of 50% is predicted in compound 1. The stretching of the OH of the molecule under study is observed at 3296 cm^{-1} (theoretical) and 3300 cm^{-1} (experimental) for compound **2**, and it is around 3279 cm^{-1} (theoretical) in compound **1**. The difference may be due to the absence of intermolecular hydrogen bonding in the gas phase. The C-N mode azo compounds are expected to appear in the region 1200 to 1300 cm^{-1}. The wave number and intensity depend on the neighboring group effect because of neighboring substituents. Strong bands appear at 1450 cm^{-1} (FT-IR) originating from the stretching vibration bands assigned to νN19-N20, which is comparable with 1453 cm^{-1} (theoretical) and with 1505 cm^{-1} in compound **1**. In compound **2**, N35-N34 stretching is predicted at 1135 cm^{-1} with TED (30%), and for compound **1**, N29-N30 is around 1063 cm^{-1}, TED (22%). C32=N34 stretching at 1600 cm^{-1} with a theoretical value of 1588 cm^{-1} for compound **2**, and for compound **1** its 1602 cm^{-1} for C27=N29 with 51% TED [34].

3.3. UV-vis data and FMO analysis

Theoretical UV-vis spectral data for compounds **1** and **2** are given in Tables 5 and 6 and Figure 3. In UV-visible data, compound **2** exhibits two transitions in water, and the one with higher oscillator strength occurs at 378.7 nm. It is due to HOMO-3 to LUMO (3%), HOMO-2 to LUMO (37%), and HOMO to LUMO (43%). In all solvents, there are two bands, one at 360-378 and 382-390 nm. The lowest wavelength 341.8 nm is obtained in water solvent [35]. Two transitions are identified in all the solvents. The highest wavelength is 360.9 nm, obtained for acetone, and the smallest is 342.6 nm for benzene solvent. It is H→L (53%) and H-1→L (41%), respectively. The experimental values coincide with the calculated λ_{max} [36]. The calculated and experimental UV visible spectral values, such as energy, oscillator strength, and λ_{max} for compound **2** are compared in Table 6. Two transitions are identified in all the solvents. The highest wavelength is 476.5 nm, obtained for DMSO, and the smallest is 396.3 nm for the benzene solvent. They are H-1→L(98) and H-1→L(88), respectively. The experimental values coincide with the calculated λ_{max} [30].

Table 4. Vibrational wavenumbers obtained for compound **2** with DFT-B3LYP/6-311+G(d,p) (Harmonic frequency (cm^{-1}), IR intensity, Raman activity (Km/mol), reduced masses (a.m.u.) and force constants (N/m)) *.

Mode No	Exp. FTIR freq. (cm^{-1})	Calc. freq. (cm^{-1})	IR intensity	Raman activity	Reduced mass	Force constant	Vibrational Assignments with >10% PED
1		3437	41.64	411.9	1.08	8.11	νN11-H12(100)
2	3307	3387	11.80	1031.4	1.08	7.87	νN35-H36(99)
3	3300	3296	509.10	313.9	1.07	7.40	νO30-H31(99)
4		3090	3.96	59.9	1.09	6.65	νC38-H41(94)
5		3087	8.46	94.3	1.09	6.65	νC4-H9(66)+νC5-H10(33)
6		3076	6.12	199.5	1.10	6.61	νC24-H29(61)+νC22-H25(38)+νC22-H25(38)
7		3073	6.01	97.7	1.09	6.56	νC4-H9(32)+νC5-H10(63)+νC5-H10(63)
8		3070	24.87	348.3	1.10	6.59	νC40-H45(11)+νC42-H46(19)+νC44-H47(67)+νC42-H46(11)
9		3068	5.13	68.1	1.09	6.57	νC1-H7(11)+νC2-H8(85)
10		3066	3.87	36.6	1.09	6.53	νC23-H27(91)
11		3063	0.20	48.4	1.09	6.51	νC24-H29(35)+νC22-H25(56)
12	3054	3054	17.35	157.6	1.09	6.50	νC40-H45(32)+νC42-H46(57)
13		3046	1.60	92.8	1.09	6.44	νC1-H7(88)+νC2-H8(11)+νC44-H47(28)+νC40-H45(53)+νC42-H46(12)
14		3029	12.81	44.9	1.09	6.37	νC39-H43(87)
15		3024	12.94	102.0	1.10	6.44	νC15-H16(32)+νC15-H18(67)
16		2992	6.23	84.2	1.10	6.26	νC15-H17(42)+νC15-H16(42)+νC15-H18(16)
17		2930	46.13	35.2	1.09	5.96	νC32-H33(100)
18		2928	2.31	223.0	1.04	5.68	νC15-H17(57)+νC15-H16(26)+νC15-H18(17)
19	1650	1677	821.14	280.2	7.32	13.14	νO14-C13(79)
20	1600	1588	89.29	951.3	5.09	8.18	νN34-C32(19)+νC28-C24(19)
21		1584	2.99	2021.5	6.26	10.02	νN34-C32(24)
22		1578	608.20	3852.0	5.40	8.58	νC5-C4(11)+νC39-C42(13)+νC39-C42(14)
23		1565	43.28	1188.2	4.85	7.59	νC44-C40(16)+νC37-C38(20)
24		1553	76.21	2584.4	4.73	7.28	νC22-C21(17)+νν34-C32(11)
25	1535	1550	111.25	195.3	5.93	9.08	νC2-C3(18)+νC6-C1(23)
26	1494	1504	183.25	154.5	2.13	3.07	βH36-N35-N34(44)+νN35-C37(10)
27		1483	96.08	4604.3	3.43	4.81	νN19-νN20(23)+νN19-N20(10)+βH10-C5-C6(14)
28		1465	114.84	452.2	2.17	2.97	βH45-C40-C44(19)+βH43-C39-C42(19)
29		1457	281.19	4862.8	3.13	4.23	νN19-N20(12)
30	1450	1453	47.09	9503.1	3.12	4.20	βH9-C4-C5(11)+νN19-N20(20)
31		1431	69.84	836.7	1.84	2.41	βH12-N11-C13(27)
32		1426	7.95	66.5	1.19	1.55	βH16-C15-H18(34)+βH18-C15-H17(24)+τH18-C15-C13-11(13)
33		1421	12.82	3163.1	2.46	3.19	βH46-C42-C44(10)+βH47-C44-C42(13)
34		1414	26.88	14.5	1.06	1.35	βH17-C15-H16(49)+βH16-C15-H18(22)
35	1406	1412	12.56	666.5	2.11	2.70	βH31-O30-C28(26)
36		1372	25.03	19.7	2.60	3.14	νC24-C22(12)+νC23-C26(15)
37	1371	1369	13.41	3514.6	2.62	3.16	βH12-N11-C13(11)+νC5-C4(10)
38		1343	122.18	57.6	1.35	1.56	βH17-C15-H16(32)+βH18-C15-H17(35)+βH16-C15-H18(14)
39		1322	25.90	6.3	1.67	1.88	βH33-C32-N34(34)
40	1300	1299	11.50	51.8	2.05	2.22	νC38-C40(12)+νC39-C42(12)+βH41-C38-C40(18)+ βH47-C44-C42(13)+βH43-C39-C42(19)
41		1291	1.07	4119.4	3.45	3.70	νC21-C23(17)
42		1280	2.97	279.1	3.76	3.95	νC4-C3(15)+νC6-C1(11)
43	1273	1270	269.15	75.7	1.87	1.94	βH8-C2-C3(11)+βH9-C4-C5(11)+βH10-C5-C6(12)
44		1268	704.33	234.1	2.36	2.44	νN11-C13(30)+νN11-C6(12)
45	1257	1252	388.93	107.0	2.99	3.01	νO30-C28(32)+βH25-C22-C24(15)
46		1237	22.81	869.5	2.94	2.88	νN19-C3(10)+νN20-C21(14)+βH33-C32-N34(11)
47		1227	334.69	2.2	2.68	2.59	νN35-C37(20)+βH36-N35-N34(11)
48		1198	25.55	556.7	2.52	2.31	νN11-C6(20)+νC6-C1(16)
49		1191	33.22	98.3	1.81	1.65	νC28-C24(13)+βH27-C23-C26(18)+βH29-C24-C22(10)
50	1171	1173	21.40	3800.3	2.26	2.00	νC26-C32(11)+νN19-C3(13)+νC28-C24(14)+βH7-C1-C2(10)
51	1153	1149	24.39	111.6	1.14	0.96	βH41-C38-C40(20)+βH45-C40-C44(18)+βH46-C42-C44(19)+ βH43-C39-C42(21)
52		1135	202.71	342.1	2.28	1.89	νN34-N35(30)
53		1131	53.55	36.9	1.23	1.01	βH45-C40-C44(15)+βH46-C42-C44(17)+βH47-C44-C42(31)
54		1124	9.64	3046.0	1.65	1.33	νN34-N35(13)+βH9-C4-C5(13)
55	1110	1108	3.52	5219.9	2.06	1.63	νN20-C21(14)+βH27-C23-C26(11)
56		1083	27.60	82.0	1.30	0.98	νC1-C2(11)+βH8-C2-C3(10)+βH25-C22-C24(13)+βH9-C4-C5(14)
57	1072	1081	68.40	1296.2	1.43	1.08	βH25-C22-C24(25)
58		1057	19.13	5.7	1.64	1.18	νC38-C40(11)+βH41-C38-C40(16)+βH47-C44-C42(16)
59	1013	1011	14.77	4.6	1.74	1.14	βH16-C15-H18(17)+τH16-C15-C13-N11(38)+τH18-C15-C13- N11(14)+YO14-C15-N11-C13(20)
60		1002	2.35	70.5	2.17	1.40	νC42-C44(28)+νC44-C40(22)
61		986	72.25	1.1	1.58	0.99	βH17-C15-H16(10)+βH18-C15-H17(12)+τH17-C15-C13-N11(30)+ τH18-C15-C13-N11(12)
62		981	1.42	46.6	2.50	1.55	βC1-C2-C3(22)+βC5-C4-C3(36)+βH8-C2-C3(10)
63	965	966	6.44	260.7	5.74	3.44	βC38-C40-C44(19)+βC42-C44-C40(20)+βC39-C42-C44(34)
64		956	7.53	32.1	3.20	1.88	νC21-C23(21)
65		951	0.30	3.6	1.33	0.77	τH9-C4-C3-C2(46)+τH10-C5-C6-N11(28)
66		950	0.13	1.5	1.28	0.74	τH45-C40-C44-C42(30)+τH46-C42-C44-C40(13)+τH47-C44-C42-C39(29)
67		933	0.11	0.1	1.33	0.74	τH29-C24-C28-C26(29)+τH25-C22-C24-C28(42)+τC28-C24-C22-C21(16)
68		931	0.74	1.2	1.35	0.75	τH7-C1-C2-C3(25)+τH8-C2-C3-C4(45)
69	922	930	0.01	0.0	1.35	0.75	τH45-C40-C44-C42(26)+τH46-C42-C44-C40(44)+ τH43-C39-C42-C44(11)+τH41-C38-C40-C44(10)
70		903	26.85	8.7	1.50	0.79	τH27-C23-C26-C28(27)+τH33-C32-N34-N35(53)
71		889	3.58	17.6	5.28	2.68	νC4-C3(18)
72		885	4.37	30.6	4.13	2.08	νC15-C13(10)+βC6-C1-C2(11)

Table 4. (Continued).

Mode No	Exp. FTIR freq. (cm^{-1})	Calc. freq. (cm^{-1})	IR intensity	Raman activity	Reduced mass	Force constant	Vibrational Assignments with >10% PED
73		873	2.78	3.9	1.43	0.70	τH27-C23-C26-C28(42)+τH33-C32-N34-N35(35)+ YC22-C23-N20-C21(11)
74		851	5.14	0.4	1.43	0.67	τH47-C44-C42-C39(33)+τH43-C39-C42-C44(24)+τH41-C38-C40-C44(30)
75	835	842	0.36	15.8	5.10	2.32	νC37-C38(10)+βC42-C44-C40(11)
76		829	52.89	4.7	1.71	0.76	τH7-C1-C2-C3(18)+τH9-C4-C3-C2(10)+τH10-C5-C6-N11(34)+ YC4-C2-N19-C3(13)
77		813	13.30	0.7	1.47	0.62	τH29-C24-C28-C26(38)+τH25-C22-C24-C28(32)+YO30-C24-C26-C28(11
78		801	3.13	13.9	1.28	0.53	τH7-C1-C2-C3(32)+τH10-C5-C6-N11(21)+τH9-C4-C3-C2(17)+τH8-C2-C3-C4(21)
79		788	0.47	0.5	1.26	0.50	τH41-C38-C40-C44(31)+τH45-C40-C44-C42(16)+ τH46-C42-C44-C40(12)+τH43-C39-C42-C44(37)
80	747	759	2.24	17.8	4.31	1.59	νC15-C13(28)
81		725	77.45	4.9	1.65	0.56	τC37-C38-C40-C44(18)+τH47-C44-C42-C39(22)+YN35-C38-C39-C37(15)
82		712	3.54	6.8	4.36	1.42	τC5-C4-C3-C2(13)+τC6-C1-C2-C3(16)
83	700	701	6.69	5.6	4.45	1.41	YO30-C24-C26-C28(19)+YC22-C23-N20-C21(10)+ τC28-C24-C22-C21(10)
84	688	682	83.04	0.4	1.23	0.37	τH31-O30-C28-C24(72)+τC37-C38-C40-C44(10)
85		669	27.30	5.4	6.48	1.86	βC24-C22-C21(13)+βC26-C32-N34(15)
86		663	3.61	0.2	1.74	0.49	τC39-C42-C44-C40(11)+τC42-C44-C40-C38(10)+ τH31-O30-C28-C24(16)+τC37-C38-C40-C44(28)
87		644	7.79	14.2	5.26	1.40	βC1-C2-C3(11)
88		625	105.12	33.4	2.06	0.52	τH12-N11-C13-C15(31)+Y O14-C15-N11-C13(32)
89		623	13.94	74.6	4.73	1.18	βC1-C2-C3(14)
90		618	9.97	27.0	6.36	1.56	βN34-N35-C37(15)+βC42-C44-C40(18)
91		605	3.72	5.5	6.38	1.50	βC37-C38-C40(11)+βC39-C42-C44(24)+βC38-C40-C44(37)
92		589	10.09	1.2	3.29	0.73	τC24-C22-C21-C23(12)+τC21-C23-C26-C32(18)+ τC3-N19-N20-C21(10)+τH25-C22-C24-C28(11)
93		546	2.67	19.1	4.74	0.91	βC3-N19-N20(10)
94		526	9.93	7.7	2.92	0.52	βO14-C13-C15(23)+YN11-C5-C1-C6(14)
95		517	62.38	48.4	4.55	0.78	βN19-N20-C21(10)+βO30-C28-C24(11)
96		502	45.44	77.0	1.88	0.30	τH18-C15-C13-N11(12)+YO14-C15-N11-C13(22)+ τH12-N11-C13-C15(35)
97		493	4.19	26.1	3.18	0.50	βO14-C13-C15(28)
98		487	21.43	0.9	2.63	0.40	τH45-C40-C44-C42(12)+τH46-C42-C44-C40(11)+ YN35-C38-C39-C37(44)+τC39-C42-C44-C40(13)
99		477	15.07	9.8	7.10	1.04	βN35-C37-C39(12)+βC37-C38-C40(16)
100		454	1.75	1.4	3.25	0.43	τH27-C23-C26-C28(13)+YO30-C24-C26-C28(17)+ YC22-C23-N20-C21(17)+τN20-C21-C23-C26(14)
101		440	4.87	41.0	5.04	0.62	βO30-C28-C24(33)
102		406	3.83	15.0	3.69	0.41	τC1-C2-C3-N19(13)+τC6-C1-C2-C3(31)+YN11-C5-C1-C6(11)
103		396	4.77	7.0	4.54	0.48	τC5-C4-C3-C2(23)+τN20-C21-C23-C26(10)
104		381	0.15	0.1	2.93	0.29	τC42-C44-C40-C38(34)+τC39-C42-C44-C40(35)+τH41-C38-C40-C44(10)
105		377	8.50	39.2	5.64	0.53	βC23-C26-C32(11)
106		376	45.42	11.9	1.43	0.13	τH36-N35-N34-C32(68)
107		376	19.29	13.9	4.09	0.37	βO30-C28-C24(11)+τH36-N35-N34-C32(13)
108		372	23.37	16.6	6.63	0.59	YC4-C2-N19-C3(10)
109		340	18.57	3.1	3.99	0.30	βN11-C6-C1(19)+βC15-C13-N11(34)
110		288	1.60	0.6	5.80	0.31	τC26-C32-N34-N35(28)+τC21-C23-C26-C32(19)+τN20-C21-C23-C26(14)
111		262	2.30	7.3	5.91	0.26	βC32-N34-N35(10)
112		233	1.78	9.8	7.13	0.25	βC22-C21-N20(10)
113		223	2.43	5.6	4.58	0.15	βC13-N11-C6(10)
114		217	8.93	4.2	3.15	0.10	τC23-C26-C32-N34(24)
115		204	1.57	4.4	5.04	0.13	τC42-C44-C40-C38(30)+YN35-C38-C39-C37(16)
116		190	5.86	1.4	5.49	0.13	τN19-N20-C21-C23(21)+τC24-C22-C21-C23(13)+τC28-C24-C22-C21(16)
117		188	8.17	28.3	5.30	0.12	βC23-C26-C32(12)+βN35-C37-C39(21)
118		177	0.68	1.3	1.12	0.02	τH16-C15-C13-N11(23)+τH17-C15-C13-N11(36)+ τH18-C15-C13-N11(12)
119		152	5.31	9.2	5.72	0.09	βC13-N11-C6(10)
120		107	2.44	2.8	6.23	0.05	τC2-C3-N19-N20(14)+τC15-C13-N11-C6(14)
121		96	0.48	0.9	5.71	0.03	τC23-C26-C32-N34(20)+τC26-C32-N34-N35(22)+τC21-C23-C26-C32(33)
122		81	3.87	1.5	6.50	0.03	τC13-N11-C6-C5(22)
123		65	0.78	0.7	6.64	0.02	τC15-C13-N11-C6(16)
124		57	0.92	7.5	6.51	0.01	βC32-N34-N35(13)+βC26-C32-N34(10)+βN34-N35-C37(12)+ τC13-N11-C6-C5(16)
125		49	4.62	12.7	3.90	0.01	βC13-N11-C6(13)+τC13-N11-C6- C5(23)+τC15-C13-N11-C6(21)
126		34	1.53	0.8	5.54	0.00	τC1-C2-C3-N19(22)+τC2-C3-N19-N20(27)
127		25	1.10	2.4	6.57	0.00	βN19-N20-C21(19)+βC3-N19-N20(16)+βC32-N34-N35(12)+ βC23-C26-C32(10)+βC26-C32-N34(10)
128		21	0.34	1.3	5.01	0.00	τN34-N35-C37-C38(61)
129		16	0.09	0.9	4.02	0.00	τN19-N20-C21-C23(23)+τC3-N19-N20-C21(10)+τC2-C3-N19-N20(19)
130		11	0.11	3.5	4.85	0.00	τC32-N34-N35-C37(60)+τC23-C26-C32-N34(19)

* ν: Stretching, β: In-plane bending, γ: Out-of-plane bending, ω: Wagging, t: Twisting, δ: Scissoring, ρ: Rocking.

3.4. Solvent effect

The molecular geometrics are obtained via DFT/6-311+G(d,p) level optimization in the gas phase and then in 9 solvents (keyword, scrf=dipole) The calculated parameters like moment, energy, hyperpolarizability, polarizability of compounds **1** and **2** in different solvents. Regular variations in energy versus dielectric constant were observed. With increasing dielectric constant of solvent, the stability of compounds **1** and **2** increases. As the dielectric constant increases, the dipole moment, hyperpolarizability, and polarizability show a regular increase, which is evident in the increased reactivity of the molecules.

Table 5. Calculated maximum absorption wavelength for compound **1**.

Solvent	Δ*E* (eV)	f (a.u.)	λ_{max} (nm)	MO contributions
Gas phase	3.2936	0.0223	376.4	H-3→L(25)
				H-2→L(41) H→L(30)
	3.6275	0.3020	341.8	H-1→L(2.9) H→L+1(92)
Benzene	3.291	0.044	376.8	H-3→L(20)
				H-2→L(40)
				H→L(36)
	3.620	0.795	342.6	H-1→L(53)
				H→L+1(41)
DCM	3.281	0.050	377.9	H-3→L(17)
				H-2→L(38)
				H→L(41)
	3.574	0.814	346.9	H-1→L(88)
				H→L+1(7)
Acetone	3.265	0.097	379.8	H-3→L(3)
				H-1→L(87)
				H→L(4)
				H→L+1(2)
	3.435	0.864	360.9	H-1→L(3)
				H→L+1(95)
Ethanol	3.276	0.050	378.5	H-3→L(16)
				H-2→L(38)
				H→L(43)
	3.563	0.792	348.0	H-1→L(89)
				H→L+1(5)
Methanol	3.276	0.049	378.5	H-3→L(16)
				H-2→L(37)
				H→L(43)
	3.565	0.785	347.8	H-1→L(89)H→L+1(5)
Acetonitrile	3.275	0.050	378.6	H-3→L(16)
				H-2→L(37) H→L(43)
	3.562	0.787	348.1	H-1→L(89)H→L+1(5)
DMSO	3.274	0.050	378.7	H-3→L(16)
				H-2→L(37)
				H→L(43)
	3.548	0.795	349.4	H-1→L(90)
				H→L+1(5)
Water	3.274	0.045	378.7	H-3→L(16)
				H-2→L(37)
				H→ (43)
	3.559	0.782	348.4	H-1→L(90)

Table 6. Calculated maximum absorption wavelength for compound **2**.

Solvent	Δ*E* (eV)	f (a.u)	λ_{max} (nm)	MO contributions	λ_{max} (nm) Exp.
Gas phase	2.811	0.352	440.9	H→L(95)	
	3.241	1.186	382.5	H→L+1(14)	
				H-1→L(83)	
Benzene	2.691	0.437	460.7	H-2→L(97)	353.68
	3.129	1.274	396.3	H-1→L(88), H→L+1(10)	
Dichloromethane	2.626	0.331	472.2	H→L(98)	
	3.115	1.376	398.0	H-1→L(88), H→L+1(10)	355.00, 239.00
Chloroform	2.649	0.361	468.1	H→L(97)	355.51
	3.120	1.346	397.4	H-1→L(88), H→L+1(10)	
Acetone	2.612	0.299	474.6	H→L(98)	
	3.120	1.396	397.5	H-1→L(97)	368.00
				H→L+1(88)	
Ethanol	2.610	0.298	475.0	H→L(98)	
	3.118	1.398	397.7	H-1→L(88)	362.53, 243.00
				H→L+1(11)	
Methanol	2.609	0.288	475.2	H→L(98)	
	3.122	1.401	397.1	H-1→L(88)	264.62, 232.00
				H→L+1(11)	
Acetonitrile	2.607	0.291	475.5	H→L(98)	
	3.120	1.402	397.5	H-1→L(88), H→L+1(11)	259.02
DMSO	2.602	0.306	476.5	H→L(98)	454.80
	3.108	1.401	398.9	H-1→L(88), H→L+1(10)	375.33
Water	2.604	0.285	476.2	H→L(98)	
	3.120	1.406	397.4	H-1→L(88), H→L+1(11)	359.18

Comparing compounds **1** and **2** with increasing dielectric constant, compound **1** exhibits a higher variation in dipole moment ranging from 5.0 to 6.8 Debye than its counterpart. Two regions of dipole moment values are identified by plotting the dipole moment μ value against the solvent's dielectric constant D, which offers light on strongly solvent-dependent molecular properties. D value ranges from 0 to 80 Debye, where the increase is seen; below the D value of zero, hardly any changes are noticed. As the dielectric constant increases, an increase in charge is expected for most of the atoms, but few atoms show a decrease in charge. In compound **1**, C1, C2, C5, N11, N14, N15, C19, C21, O25, and N30, in compound **2**, C2, C4, C6, C15, N19, N20, O30, N34, and N39, atoms found to have decreased charge although the dielectric constant increased.

Table 7. Mulliken atomic charges and natural population analysis by B3LYP/6-311+G(d,p) method for compounds **1** and **2**.

Atom	Compound 1		Atom	Compound 2	
	Mulliken atomic charge	NPA		Mulliken atomic charge	NPA
C1	0.0776	-0.263	C1	-0.2734	-0.226
C2	-0.1758	-0.145	C2	-0.1438	-0.163
C3	-0.4218	0.044	C3	-0.2890	0.088
C4	0.1519	-0.165	C4	0.0136	-0.178
C5	-0.1577	-0.247	C5	-0.0007	-0.224
C6	-0.1485	0.189	C6	0.0923	0.164
H7	0.1084	0.205	H7	0.1232	0.211
H8	0.1329	0.222	H8	0.1326	0.220
H9	0.1441	0.229	H9	0.1531	0.232
H10	0.1084	0.204	H10	0.1253	0.213
N11	-0.3598	-0.779	N11	-0.2004	-0.631
H12	0.2335	0.379	H12	0.2808	0.403
H13	0.2337	0.379	C13	0.0800	0.687
N14	0.1823	-0.168	O14	-0.3184	-0.613
N15	0.0852	-0.220	C15	-0.3834	-0.673
C16	-0.5492	0.097	H16	0.1656	0.220
C17	0.2179	-0.189	H17	0.1713	0.226
C18	-1.0616	-0.180	H18	0.1798	0.236
C19	-0.0160	-0.240	N19	0.0768	-0.231
H20	0.1179	0.213	N20	0.0539	-0.228
C21	0.7960	-0.157	C21	-0.6864	0.162
H22	0.1077	0.209	C22	0.2931	-0.180
C23	-0.1559	0.347	C23	-0.4731	-0.186
H24	0.1291	0.219	C24	-0.2102	-0.258
O25	-0.3579	-0.691	H25	0.1354	0.220
H26	0.3923	0.502	C26	0.8095	-0.164
C27	-0.0706	0.052	H27	0.1409	0.226
H28	0.1307	0.182	C28	-0.3002	0.375
N29	-0.1498	-0.317	H29	0.1338	0.224
N30	-0.0070	-0.404	O30	-0.3404	-0.675
H31	0.2480	0.377	H31	0.3928	0.503
C32	-0.0130	0.126	C32	-0.0619	0.059
C33	0.2478	-0.220	H33	0.0822	0.167
C34	-0.2510	-0.222	N34	0.0489	-0.395
C35	-0.1483	-0.192	N35	-0.1113	-0.381
H36	0.1418	0.219	H36	0.2670	0.364
C37	-0.2671	-0.191	C37	-0.6068	0.159
H38	0.1192	0.208	C38	0.9359	-0.245
C39	-0.1863	-0.210	C39	-0.4175	-0.244
H40	0.1306	0.210	C40	-0.4329	-0.176
H41	0.1309	0.210	H41	0.1249	0.217
H42	0.1294	0.209	C42	-0.2233	-0.183
			H43	0.1027	0.202
			C44	-0.0238	-0.237
			H45	0.1295	0.208
			H46	0.1274	0.208
			H47	0.1248	0.209

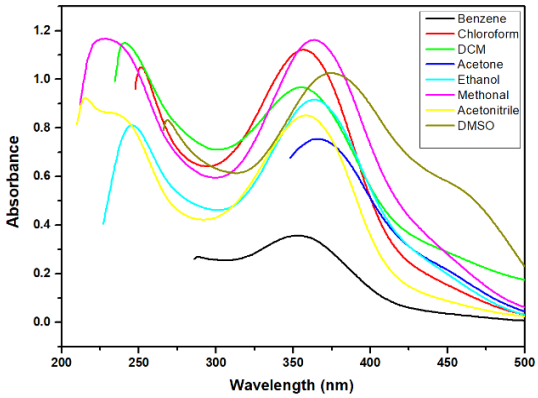

Figure 3. Absorption spectra of compound **2** in different solvents.

The stability of compounds **1** and **2** increases with increasing dielectric constants; comparatively, compound **2** enjoys more stability than compound **1** [37].

Compound **1** exhibits maximum polarizability in water 11.2314, followed by DMSO 11.1825, which follows an order with respect to dielectric constant. As the dielectric constant increases, the polarizability also increases. In compound **2** also, the same trend is identified, that maximum is shown in water followed by DMSO. These molecules exhibit polarizability comparable to diethylamine and are candidates for a good electro-optic response [38]. Hyperpolarizability: On studying the hyperpolarizability values of compound **1**, it is observed that the compound under study shows a maximum first-order hyperpolarizability of 5.00783×10^{-30} e.s.u. in water. An increasing trend of hyperpolarizability is observed as an increase in the dielectric constant.

Table 8. Second-order perturbation theory analysis of Fock-Matrix in NBO basis for compound **1**.

Donor	Occupancy	Acceptor	$E^{(2)}$, kcal/mol	E_j-E_i, a.u.	F(*i,j*), a.u.
πC1-C2	1.9724	LP(1)C3	37.77	0.15	0.085
πC1-C2	1.9724	LP*(1)C6	56.45	0.14	0.096
πC4-C5	1.9725	LP(1)C3	37.02	0.15	0.085
πC4-C5	1.9725	LP*(1)C6	52.13	0.14	0.093
πN14-N15	1.9875	LP(1)C3	14.92	0.26	0.079
πC16-C18	1.9682	π*C17-C19	20.37	0.29	0.069
πC16-C18	1.9682	π*C21-C23	17.06	0.28	0.064
πC17-C19	1.9708	π*C16-C18	18.53	0.29	0.066
πC17-C19	1.9708	π*C21-C23	21.69	0.28	0.072
πC21-C23	1.9722	π*C27-N29	21.19	0.29	0.071
πC21-C23	1.9722	π*C17-C19	16.76	0.29	0.063
πC21-C23	1.9722	π*C27-N29	20.02	0.25	0.066
πC32-C34	1.9757	π*C33-C35	18.88	0.29	0.066
πC32-C34	1.9757	π*C37-C39	20.46	0.29	0.069
πC33-C35	1.9770	π*C32-C34	20.97	0.28	0.069
πC33-C35	1.9770	π*C37-C39	19.13	0.28	0.066
πC37-C39	1.6643	π*C32-C34	20.00	0.28	0.067
πC37-C39	1.6643	π*C33-C35	20.97	0.28	0.069
LP(1)C3	1.9992	π*C1-C2	75.30	0.14	0.110
LP(1)C3	1.9992	π*C4-C5	70.45	0.14	0.108
LP(1)C3	1.9992	π*N14-N15	66.54	0.10	0.091
LP*(1)C6	1.9991	π*C1-C2	53.19	0.15	0.100
LP*(1)C6	1.9991	π*C4-C5	50.19	0.15	0.099
LP(1)N11	1.9660	LP*(1)C6	58.89	0.18	0.117
LP(2)O25	1.9612	π*C21-C23	32.36	0.33	0.100
LP(1)N30	0.0030	π*C21-C23	25.30	0.30	0.078
LP(1)N30	0.0030	π*C27-C29	13.39	0.31	0.060
π*C21-C23	0.0294	π*C16-C18	263.14	0.01	0.078
π*C27-C29	0.0419	π*C21-C23	80.67	0.03	0.072

Maximum hyperpolarizability is observed in a water solvent for compound **2**. Compound **2** also shows an increase in hyperpolarizability as the value of the dielectric constant increases. Compounds **1** and **2** in various solvents exhibit hyperpolarizability values higher than urea 0.65×10^{-30} e.s.u. When comparing compounds **1** and **2**, the maximum value is identified in compound **1** (7.17672 Debye). Both compounds in water show maximum hyperpolarizability, dielectric constant, dipole, and deficient energy, indicating better NLO properties [39].

3.5. Mulliken charges

Mulliken charge calculation is important in quantum chemistry because it affects the electronic structure, molecular polarization, dipole moment, and many molecular properties. The distribution of charge in an atomic molecule is determined by the donor and acceptor pairs of electrons. Atomic charge is used in electronegativity processes, equalization, and charge transmission in chemical reactions [40-42]. The calculated Mulliken atomic charge by the DFT method on the basis set B3LYP/6-311+G(d,p) is shown in Table 7. It is notable that in compound **1**, the atoms C1, C4, N14, N15, C17, C21 and C4, C6, C13, N19, N20, C22, C26 in compound **2** exhibit a positive charge. Negative charge is found on the atoms C2, C3, C5, C6, N11, C16, C18, C19, C23, O25, C27, N29, N30, C32 andC1, C2, C3, C5, N11, O14, C15, C21, C23, C24, C28, O30, C32 with respect to compounds **1** and **2** [35]. The maximum positive charge is exhibited by C21 on compound **1** and C26 on compound **2** and is attributed to the presence of a hydroxyl group adjacent to carbon and attachment of imine carbon directly on C21and C26. The maximum positive charge is due to the electron-withdrawing effect of oxygen and nitrogen, as well as the orientation of the atoms.

An excess of electrons is seen on C18, C16 in compound **1**, C21 and C23 in their counterparts. This negative charge accumulation may be due to the π channel and the push-pull mechanism of the electrons. An excess of negative charge is identified on C18, C6, C2, C3, C16, C17, C19, and C23, which is due to the π-conjugation of electrons from nitrogen in compound **1**. This charge is reversed in compound **2**, and hence, the reverse of the nucleophilic and electrophilic centers in compound **2**. The reverse of charge accounted for is due to the anilide functional in place of the aniline group. On comparing Mulliken and NPA analyses, the results obtained are comparable with a few exceptions. H26 in compound **1**, H31 in compound **2** show higher positive charge (0.3923) Mulliken, (0.502) NPA, and (0.3928) Mulliken, (0.503) NPA, respectively [43]. This is due to the electronegativity of O26 and O30 in the respective compounds and also to the hydrogen bonding interaction between O25-H26···N29 in compound **1** and O30-H31···N34 in compound **2**. The intramolecular interaction is supported by an increase in C=N bond length and a decrease in the C=N stretching frequency. C27-N29 (1.294 Å, 1602 cm^{-1}), C32-N34 (1.2936 Å, 1588 cm^{-1}), and also decreased in O-H stretching frequency (O25-H26 3279 cm^{-1}), (O30-H31 3296 cm^{-1}) in compounds **1** and **2**, respectively.

3.6. NBO analysis

The second-order Fock matrix evaluated donor-acceptor interactions on the basis of NBO [44]. The interactions result in a loss of occupancy from the localized NBO of the idealized Lewis structure into an empty non-Lewis orbital. For each donor (*i*) and acceptor (*j*), the stabilization energy $E^{(2)}$ associated with the delocalization *i-j* is estimated [45].

In the NBO analysis, a large value of $E^{(2)}$ shows the intensive interaction between electron donors and electron acceptors and the greater degree of conjugation in the whole system (Tables 8 and 9). π*C21-C23 to π*C16-C18 and π*C27-C29 to π*C21-C23 are intensive interactions in compound **1** and in compound **2** it is found to be π*C1-C6 to π*C4-C5 and π*C37-C38 to π*C40-C44. Between the two molecules under study, compound **1** shows the strongest interaction.

Intramolecular hyperconjugative interactions are formed by orbital overlap between the π(C-C) bonding molecular orbital and the π*(C-C) anti-bonding molecular orbital of the phenyl ring of the title molecule [46,47]. For compound **1** donors, C16-C18, C16-C18, C17-C19, C17-C19, C21-C23, C21-C23, C32-C34, C32-C34, C33-C35, C33-C35, C37-C39, C37-C39, the corresponding acceptors are C17-C19, C21-C23, C16-C18, C21-C23, C27-N29, C17-C19, C27-N29, C33-C35, C37-C39, C32-C34, C37-C39, C32-C34, C33-C35, and their second order perturbation energy values are 20.37, 17.06, 18.53, 21.69, 21.19,

Table 9. Second-order perturbation theory analysis of Fock-Matrix in NBO basis for compound **2.**

Donor	Occupancy	Acceptor	$E^{(2)}$, kcal/mol	E_j-E_i, a.u.	F(*i*,*j*), a.u.
πC1-C6	1.6439	π*C2-C3	21.93	0.29	0.072
πC1-C6	1.6439	π*C4-C5	16.76	0.29	0.064
πC2-C3	1.6087	π*C1-C6	20.19	0.27	0.066
πC2-C3	1.6087	π*C4-C5	20.40	0.28	0.070
πC2-C3	1.6087	π*N19-N20	20.03	0.24	0.064
πC4-C5	1.6949	π*C1-C6	21.41	0.28	0.070
πC4-C5	1.6949	π*C2-C3	17.42	0.29	0.064
πN19-N20	1.9148	π*C2-C3	10.54	0.39	0.062
πC21-C23	1.6119	π*N19-N20	16.67	0.23	0.058
πC21-C23	1.6119	π*C22-C24	21.27	0.28	0.070
πC37-C38	1.6404	π*C39-C42	16.89	0.29	0.063
πC37-C38	1.6404	π*C40-C44	22.24	0.30	0.073
πC39-C42	1.7080	π*C37-C38	21.31	0.28	0.071
πC39-C42	1.7080	π*C40-C44	16.18	0.30	0.063
πC40-C44	1.6673	π*C37-C38	19.21	0.27	0.066
πC40-C44	1.6673	π*C39-C42	22.69	0.28	0.071
LP(1)N11	1.6872	π*C1-C6	23.16	0.28	0.073
π*C1-C6	0.38987	π*C4-C5	235.93	0.01	0.081
π*C37-C38	0.40980	π*C40-C44	215.16	0.01	0.081

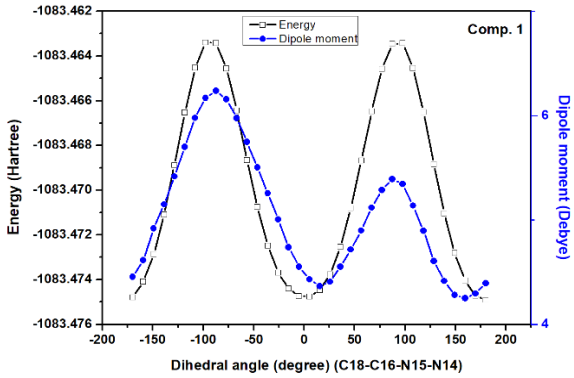

Figure 4. Energy, dipole moment versus dihedral angle of compound **1.**

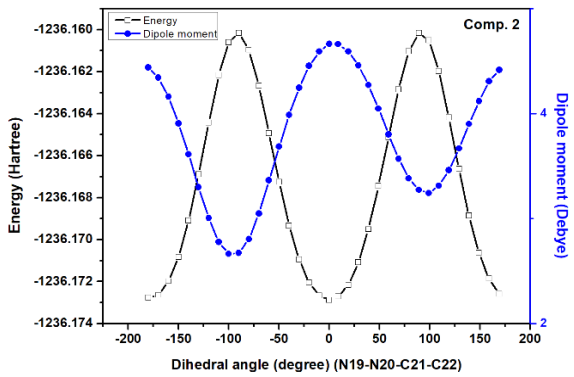

Figure 5. Energy, dipole moment versus dihedral angle of compound **2.**

16.76, 20.02, 18.88, 20.46,20.97, 19.13, 20.0, and 20.97 kcal/mol. Similarly for compound **2** the donors are C1-C6, C1-C6, C2-C3, C2-C3, C4-C5, C4-C5, N19-N20, C21-C23, C21-C23, C37-C38, C37-C38, C39-C42, C39-C42, C40-C44, C40-C44 the corresponding acceptors are C2-C3, C4-C5, C1-C6, C4-C5, N19-N20, C1-C6, C2-C3, C2-C3, N19-N20, C22-C24, C39-C42, C40-C44, C37-C38, C39-C42 and their second-order perturbation values are 21.93, 16.76, 20.19, 20.4, 20.03, 21.41, 17.42, 10.54, 16.67, 21.27,16.89, 22.24, 21.31, 16.18, 19.21, and 22.69 kcal/mol.

3.7. Dihedral angle studies

3.7.1. Potential energy

The variation in energy and dipole moment of compounds **1** and **2** as a function of dihedral angle are shown in Figures 4 and 5. It is evident from Figure 4 that the conformers having a dihedral angle of -170, -5, 5, or 180° are stable ones with minimum energy in the case of compound **1** and it is due to the relaxed dihedral angle that places all the phenyl rings in a plane parallel to one another. In compound **2,** the conformers with dihedral angles 0, 180, 9, -10, and -170° exhibit minimum energy and enjoy better stability because all three rings are in the plane. In compounds **1** and **2**, the conformers with the phenyl ring perpendicular to their counterparts experience more strain, and they are explicitly less stable with high energy. The conformers with less stability are dihedral angles -97, 97, -87, 87, -108° and 99, -99, 89, 100, -80° in compounds **1** and **2**, respectively [25,48].

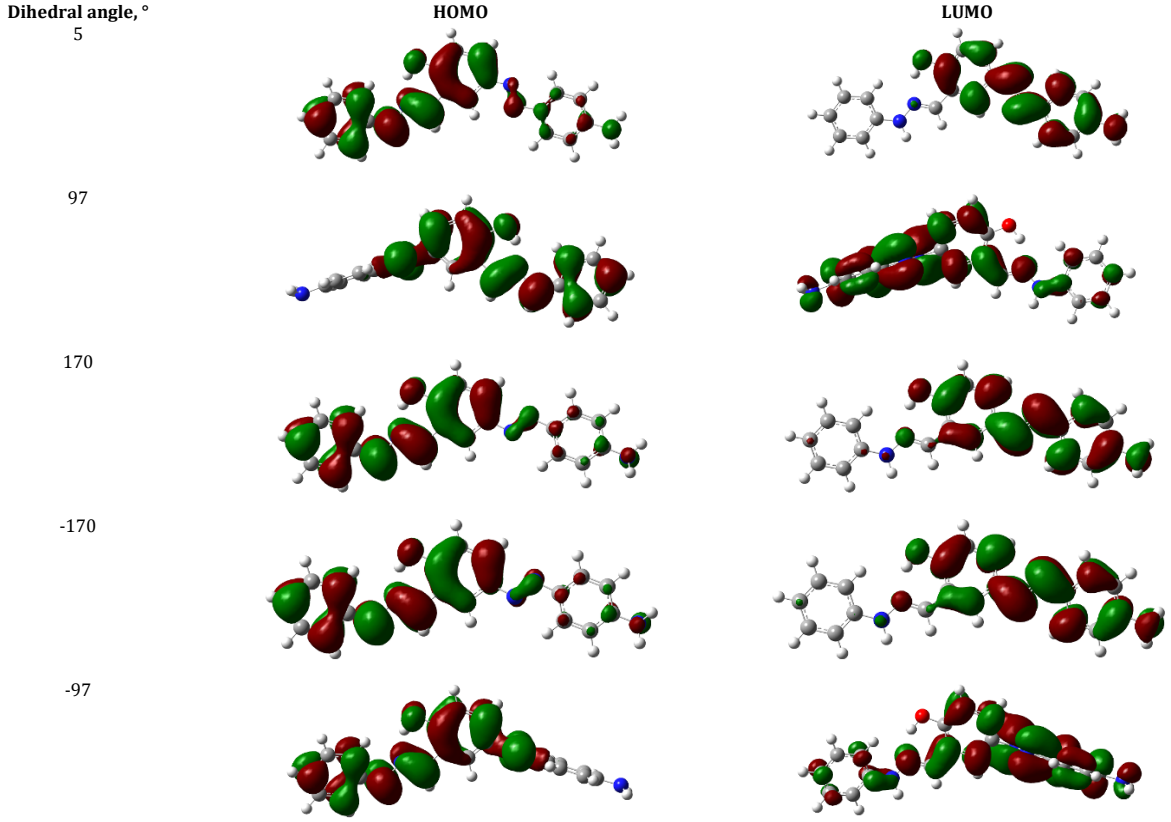

Figure 6. HOMO-LUMO diagrams of compound **1** at various dihedral angles.

3.7.2. Dipole moment

The variation in energy and dipole moment of compounds **1** and **2** as a function of dihedral angle are shown in Figures 4 and 5. It is evident from the figure that as the dihedral angle increases, energy and dipole moment also increase and reach a maximum of 6.237 Debye at -87°, at which the aniline moiety is perpendicular to the phenoxy moiety. The dipole moment decreases as the dihedral angle increases further and reaches a second maximum of 5.390 Debye at 87°. The dipole moment is at its minimum whenever the molecule reaches a planar structure with minimal energy and stable configuration in compound **1**. In contrast, the dipole moment reaches a maximum of 4.662 Debye at a dihedral angle of 0° and an energy minimum. Energy and dipole moment are inversely related in compound **2**; the dihedral angle at which the maximum energy is obtained becomes the minimum for the dipole moment and vice versa [25]. This behavior is notably different from compound **1.**

3.7.3. HOMO-LUMO, hardness, electrophilicity

In compound **1**, Δ*E*, the hardness and electrophilicity index of the compound are compared with dihedral angles at -170, 0, and 180°. The energy gap is found to be a minimum of 2.0812929 eV at -170°, which is found to be the most stable conformer with minimum energy. The molecule exhibits a maximum hardness of 1.7189918 at a dihedral angle of -97° and a conformer with maximum energy and minimum stability [48-50]. At 97 °, the energy is at its peak and the electrophilicity index is found to be at its maximum point for compound **1**. In compound **2**, Δ*E*, the hardness and electrophilicity index of the compound are compared with dihedral angles at -170, -100, 1, 100, and 170°. The energy gap is found to be minimum 1.997214 eV at 170°, which is found to be a stable conformer with minimum energy and maximum dipole moment and also maximum hardness 1.5723, is recorded at the same point. At -100°, the energy is found to be maximum, the dipole is minimum, and the electrophilicity index is found at the maximum point for compound **2**. When comparing the HOMO-LUMO diagrams (Figures 6 and **7**) of compounds **1** and **2** at various dihedral angles, there is some similarity with the distribution of HOMO-LUMO orbitals at similar dihedral angles. The distribution of HOMO orbitals in compound **1** at 5° is mainly on ring 3 (phenylhydrazone moiety) and ring 2 (phenoxymoiety). When the angle changes to 97° the HOMO orbitals retain the position with respect to ring 2 and 3, but no lobe is identified on ring 1 (aniline moiety). The HOMOs at dihedral angles 5, 170, and -170° are similar with a difference in positive and negative charges. The HOMO of compounds **1** at 97° and -97° exhibits similar orbital orientations [51,52]. Planar geometry gives an extended conjugation throughout the chain and leads to a strong delocalization of holes in the HOMO [53]. LUMO of compound **1** at a dihedral angle of 5°, the lobes are located on ring 1 and ring 2 only; as the angle increases to 97° and to 170°, the lobe is red, which is a tribute to the azo group, and a little on ring 1. At dihedral angles of 170° and -170°, the lobes are similar with opposite charge distribution. At dihedral angles 0, 100, 170, -170, and -100°, the HOMO of compound **2** is densely distributed on ring 2 (phenoxymoiety) and ring 3 (phenylhydrazone moiety); on the contrary, LUMO at the dihedral angles mentioned above is solidly identified on ring 1(acetanilidemoiety). The energy gap (Δ*E*) of compound **1** is found to be minimum at angle -170° and 0° in compound **2** and is found to be -1083.474796 and -1236.172885, respectively.

3.8. FMO properties

The global reactivity descriptors such as chemical potential, electronegativity, hardness, softness, electrophilicity index, and local reactivity descriptors such as Fukui functions can be calculated using DFT.

Table 10. HOMO and LUMO energy, chemical potential, hardness and electrophilicity index calculated by B3LYP/6-311+G(d,p) method for compounds **1** and **2.**

Parameters	Compound 1	Compound 2
E_{HOMO} (eV)	-5.51	-5.74
E_{LUMO} (eV)	-1.93	-2.58
E_{LUMO}-E_{HOMO} (eV)	3.58	3.16
Electronegativity (eV)	-3.72	-4.16
Hardness (eV)	1.79	1.58
Electrophilicity index (eV)	3.865	5.476
Softness (1/eV)	0.279	0.316

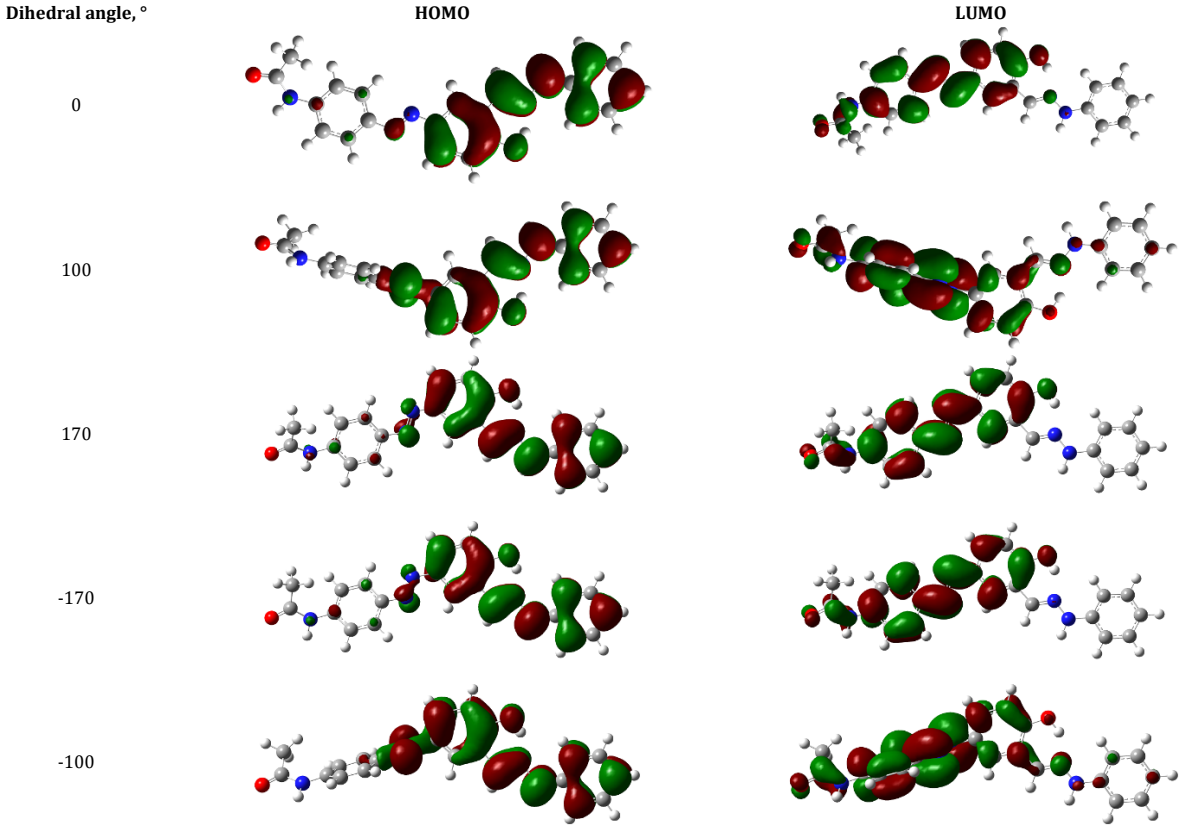

Figure 7. HOMO-LUMO diagrams of compound **2** at various dihedral angles.

The calculation procedure was illustrated and the values are listed in Table 10 [53]. The inverse of hardness is expressed as the global softness S=(1/2η). The global electrophilic index ($\omega = -\mu^2/2\eta$) assesses the lowering of energy due to the maximal electron flow between donor and acceptor. The highest occupied molecular orbital (HOMO) and the lowest unoccupied molecular orbital (LUMO) are vital parameters for quantum chemistry. We can determine how the molecule interacts with other species; hence, these are called the frontier orbitals. HOMO, which can be thought of as the outermost orbital containing electrons, tends to give these electrons as an electron donor.

In contrast, LUMO is the innermost orbital, containing free orbitals to accommodate electrons [54]. The values of electro-negativity, chemical hardness, softness, and electrophilicity index for compounds **1** and **2** are given in Table 10**.** When the chemical hardness is considered, if one molecule has a large HOMO-LUMO gap, then it is a hard molecule and vice versa. If a molecule exhibits the least HOMO-LUMO gap, it is more reactive and softer [55,56]. In compound **1**, Figure 8**,** HOMO is concentrated on the two azo nitrogen atoms, and LUMO is spread over the phenoxy ring and the amine ring. On the contrary, the HOMO in compound **1** is spread over the phenyl hydrazone moiety, the phenoxy moiety, and the LUMO exactly on the other side of the molecule. The energy difference between HOMO and LUMO is found to be 3.58 and 3.16 eV in **1** and **2**, respectively, from which we argue for the enhanced reactivity of the molecules. The molecule with the lowest band gap (G) happens to be the one with the highest polarizability and dipole moment. It also has the highest molecular size and the highest planarity. This means that the molecule is the most reactive and polarizable, has the highest electro-optic response, and is the softest [56]. Compound **2,** with a minimum band gap, is more reactive; it is a soft molecule with several transitions. Electronic communication between the donor and acceptor increases when the band gap decreases and is expected to increase more in compound **2**. This minimum band gap in compound **2** can be attributed to increased conjugation throughout the molecule. Compound **1** exhibits a dipole moment of 4.99 and a polarizability of 8.2, which is comparable to its counterpart, and exhibits a planar structure, which enhances the reactivity of the molecule [54,56].

3.9. Aromaticity indices

The neutral and cation of compound **2** show a significant negative NICS value (Table 11), a more quantitative measure of the aromatic character than the anion. The maximum negative value is observed for 1.5 Bq -1 Bq (Distance of NICS probe from molecular plane–Bq) below and above the ring (zz) for the neutral moiety.

Table 11. DFT-B3LYP/6-311+G (d,p) method calculated NICS (ppm) values (neutral, cation and anion) for compound **2.**

Bq	NICS RING 1 (Anilide ring)					
	Neutral		Cation		Anion	
	Isotropic	Anisotropic (zz)	Isotropic	Anisotropic (zz)	Isotropic	Anisotropic (zz)
-0.2	-0.3839	-11.8430	-3.3091	-11.4238	-3.2921	-10.9051
-1.5	-5.3173	-17.0004	-4.9950	-14.7632	-6.1115	-13.5677
-1.0	-7.6962	-21.4586	-6.3111	-14.3814	-7.9417	-11.2753
-0.5	-8.6099	-18.5047	-5.2637	-4.9876	-5.5897	-3.0289
0.0.	-7.3079	-8.2208	-3.6440	-2.8604	-4.0690	-0.3804
0.5	-0.0707	-11.0826	-5.2623	-5.5617	-7.1566	-5.6186
1.0	-9.3235	-21.5428	-6.1317	-14.3799	-8.8005	-13.2548
1.5	-7.6032	-21.8350	-4.8235	-14.4762	-6.1009	-13.7072
2.0	-5.0239	-16.4992	-3.2216	-11.1855	-3.2095	-10.2785
Bq	**NICS RING 2 (Hydroxy ring)**					
	Neutral		Cation		Anion	
	Isotropic	Anisotropic (zz)	Isotropic	Anisotropic (zz)	Isotropic	Anisotropic (zz)
-0.2	-3.5505	-12.1407	-2.6422	-8.9955	-2.7917	-9.8515
-1.5	-5.6016	-16.8520	-3.8435	-10.6828	-4.3876	-12.6808
-1.0	-7.9255	-19.8116	-4.5803	-8.3668	-5.7799	-11.8673
-0.5	-8.4751	-14.2765	-3.3375	-1.6205	-5.2343	-2.3546
0.0	-7.1238	-4.4661	-1.8551	-9.1358	-4.2096	-4.8613
0.5	-7.9439	-9.9574	-3.3500	-1.5552	-5.4768	-4.1639
1.0	-8.4479	-19.1311	-4.5773	-8.3950	-5.7081	-12.4506
1.5	-6.5302	-18.5908	-3.8336	-10.676	-4.1676	-12.3699
2.0	-4.2568	-13.9636	-2.6344	-8.9805	-2.6092	-9.4348
Bq	**NICS RING 3 (Phenylhydrazine ring)**					
	Neutral		Cation		Anion	
	Isotropic	Anisotropic (zz)	Isotropic	Anisotropic (zz)	Isotropic	Anisotropic (zz)
-0.2	-4.7384	-16.6854	-3.8708	-13.9433	-3.3201	-12.7870
-1.5	-7.3909	-22.5985	-6.0855	-19.0217	-5.6439	-18.2701
-1.0	-9.4836	-23.9394	-8.1244	-20.9990	-8.4273	-22.3315
-0.5	-8.7217	-14.5558	-7.6335	-13.1713	-9.1009	-17.9314
0.0	-7.9596	-9.8057	-6.0488	-4.7996	-7.1777	-7.1552
0.5	-9.5357	-20.3063	-7.6089	-13.0472	-8.0861	-11.4971
1.0	-8.6674	-24.2909	-8.1301	-20.9675	-9.3656	-21.1402
1.5	-5.9230	-19.5300	-6.1079	-19.0613	-7.4661	-21.2954
2.0	-3.6275	-13.6450	-3.8897	-13.0223	-4.6972	-16.1272

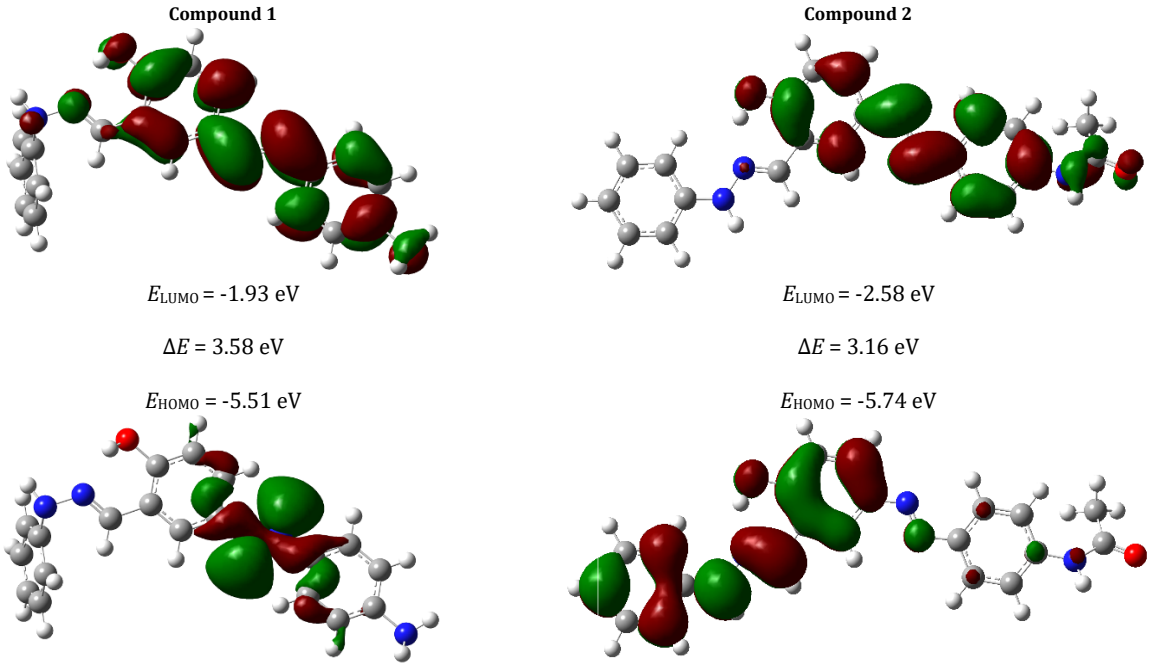

Figure 8. HOMO-LUMO of compounds **1** and **2.**

The decreasing order of NICS is neutral > cation > anion. However, in ring 2 (phenoxy ring), neutral and anions have a more considerable NICS negative value than the cation. The maximum negative value is obtained for -1Bq and 1Bq in neutral species below and above the ring (zz). The NICS order is cation<anion<neutral. In ring 3, the neutral and anion show a more significant negative value than the cation. The maximum negative value for 1 Bq and -1 Bq above and below the ring in the neutral species is observed. The order of the NICS value is cation<anion<neutral. The NICS value of ring 1 differs from the order of the NICS value of ring 2 and ring 3, and this may be attributed to the occupancy of HOMO and LUMO in the molecule in different ionic states of the candidate molecule. The HOMO is more contributed by the azo group than by the rest of the molecule, and this is realized in the NICS value. LUMO, which is contributed by rings 1 and 2, shows its efficacy in accepting any number of electrons, leading to a decrease in the NICS value [57,58].

Table 12. Calculated local reactivity properties of compound **1** using B3LYP/6-311+G(d,p) method for Mulliken derived charges.

Atoms	f_k^+	f_k^-	$\Delta f_k(r)$	S_k^+	S_k^-	S_k^+/S_k^-	$\Delta S_k(r)$	ω_k^+	ω_k^-	$\Delta\omega_k(r)$
C1	0.0364	-0.0610	0.0974	0.0102	-0.0170	-0.5976	0.0272	0.1990	-0.3330	0.5320
C2	-0.0928	0.1705	-0.2633	-0.0259	0.0476	-0.5439	-0.0735	-0.5066	0.9314	-1.4381
C3	-0.0580	0.1056	-0.1636	-0.0162	0.0295	-0.5492	-0.0457	-0.3168	0.5768	-0.8936
C4	0.1505	-0.0863	0.2368	0.0420	-0.0241	-1.7429	0.0661	0.8219	-0.4716	1.2935
C5	0.0079	-0.0791	0.0870	0.0022	-0.0221	-0.1002	0.0243	0.0433	-0.4319	0.4752
C6	0.0688	0.1705	-0.1017	0.0192	0.0476	0.4035	-0.0284	0.3758	0.9313	-0.5555
N11	0.0379	-0.0036	0.0416	0.0106	-0.0010	-10.451	0.0116	0.2072	-0.0198	0.2271
N14	0.0874	-0.0527	0.1401	0.0244	-0.0147	-1.6575	0.0391	0.4772	-0.2879	0.7650
N15	0.1099	-0.0439	0.1538	0.0307	-0.0122	-2.5069	0.0430	0.6005	-0.2395	0.8400
C16	0.0638	-0.0858	0.1496	0.0178	-0.0240	-0.7433	0.0418	0.3484	-0.4687	0.8171
C17	0.0268	0.0960	-0.0692	0.0075	0.0268	0.2793	-0.0193	0.1464	0.5242	-0.3778
C18	-0.0425	0.0228	-0.0653	-0.0119	0.0064	-1.8641	-0.0182	-0.2321	0.1245	-0.3566
C19	-0.0135	-0.2796	0.2660	-0.0038	-0.0781	0.0484	0.0743	-0.0739	-1.5270	1.4531
C21	0.0104	-0.0365	0.0469	0.0029	-0.0102	-0.2857	0.0131	0.0570	-0.1994	0.2563
C23	0.0483	0.3057	-0.2574	0.0135	0.0854	0.1580	-0.0719	0.2639	1.6700	-1.4061
O25	0.0295	0.0727	-0.0432	0.0082	0.0203	0.4059	-0.0121	0.1612	0.3972	-0.2360
C27	0.0462	0.0810	-0.0348	0.0129	0.0226	0.5702	-0.0097	0.2524	0.4427	-0.1903
N29	0.0416	0.1355	-0.0939	0.0116	0.0378	0.3072	-0.0262	0.2274	0.7400	-0.5127
N30	-0.0117	-0.1133	0.1016	-0.0033	-0.0317	0.1030	0.0284	-0.0638	-0.6190	0.5552
C32	0.0579	0.1506	-0.0927	0.0162	0.0421	0.3846	-0.0259	0.3164	0.8225	-0.5062
C33	-0.0130	0.0872	-0.1002	-0.0036	0.0243	-0.1490	-0.0280	-0.0709	0.4762	-0.5471
C34	-0.0103	-0.1731	0.1628	-0.0029	-0.0483	0.0594	0.0455	-0.0562	-0.9455	0.8893
C35	0.0271	-0.0059	0.0329	0.0076	-0.0016	-4.6143	0.0092	0.1478	-0.0320	0.1799
C37	0.0079	0.0664	-0.0585	0.0022	0.0186	0.1194	-0.0163	0.0433	0.3629	-0.3196
C39	0.0281	-0.0021	0.0302	0.0079	-0.0006	-13.713	0.0084	0.1537	-0.0112	0.1649

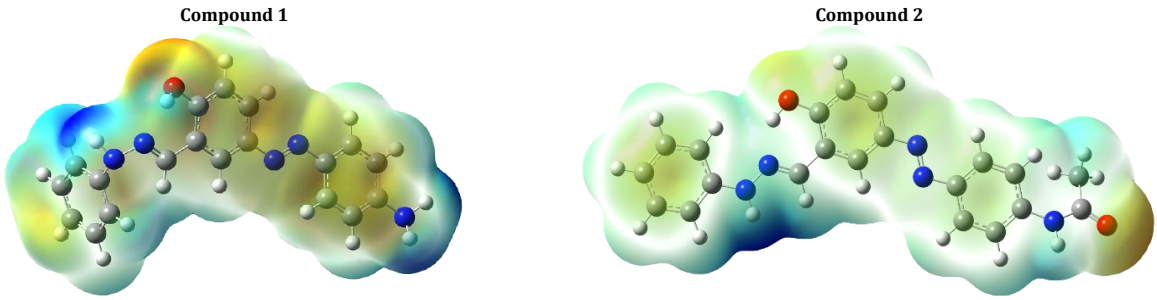

Figure 9. MEP of compounds **1** ($-9.48e^{-2}$ – $9.48e^{-2}$) and **2** ($-6.322e^{-2}$ – $6.322e^{-2}$).

3.10. HOMA

In the neutral state, the HOMA value for compounds **1** and **2**, and all three rings is 0.9874. In the anionic state, the HOMA value follows the order ring 3 > ring 1 > ring 2 in compounds **1** and **2**. Compound **1** shows a higher HOMA value than compound **2** in the anionic state when comparing rings 1 and 3. The hydroxyl ring (ring 2) in compound **2** produces 0.9201, compared to 0.8742 in ring 2 in compound **1**. In the cationic state, compound **1** exhibits the same HOMA value for ring 1 and ring 2, and is higher compared to the value of ring 3. On the contrary, in compound **2**, ring 3 shows a higher HOMA value, followed by ring 1 and ring 2. When the neutral state is excluded from all other states stated in compound **2**, ring 2 shows a lower HOMA value than its counterpart. This is evident in the less aromatic character of ring 2, which is also supported by the orientation of LUMO to the hydroxyl ring and the lower NICS value [59].

3.11. Fukui function

A molecule is susceptible to nucleophilic attack at sites where f_k^+ is large. Similarly, a molecule is susceptible to electrophilic attack at sites where f_k^- is large, because these are the regions where electron removal destabilizes the molecule the least [60]. The calculated values of the Fukui function are presented in Tables 12 and 13. In compound **1**, the increasing order of nucleophilic attack is C37 < C5 < C21 < C17 < C35 < C39 < O25 < C1 < N11 < N29 < C27 < C23 < C32 < C16 < C6 < N14 < N15 < C4. C4 carbon is more prone to nucleophilic attack. C23 in compound **1** is found to be the most reactive site to electrophiles [61]. The decreasing order of electrophilic attack is C23 > C2 > C6 > C32 > N29 > C3 > C17 > C33 > C27 > O25 > C37 > C18. In compound **2** the increasing order of nucleophilic attack is C40 < C42 < C44 < C5 < C3 < C24 < C38 < C4 < C21 < C6. C6 and C21, which are directly attached to the anilide and azo groups, are deficient in electron density and prone to nucleophilic attack [61]. The order of electrophilic attack is found to be C22 > C2 > C28 > C3 > C44 > C39 > C40 > C38 > C26 [62].

3.12. MEP

The MEP surface throws light on the reactivity of a molecule in that the negative region is prone to electrophilic sites, while the positive region is a nucleophilic site [63,64]. In Figure 9, the electrophilic region is shown as the negative region (red color) region, and the nucleophilic center is shown as the positive region (blue color) region of MEP. The potential increases as the color changes from red, orange, yellow, green, and blue. The negative potential for compound **1** starts at -9.48×10^{-2} and is distributed over the phenyl rings 1 and 2. It may be due to delocalization of π-electrons and is prone to electrophilic attack. The regions near nitrogen are blue, which is not a preferable site for an electrophilic attack. In compound **2**, the negative potential starts at -6.33×10^{-2} and is found in the aromatic system. This may be due to the π-electron density. These are sites for electrophilic attack. Furthermore, the blue regions near nitrogen are less favourable for electrophilic attack [56,65].

Table 13. Calculated local reactivity properties of compound **2** using B3LYP/6-311+G(d,p)method for Mulliken derived charges.

Atoms	f_k^+	f_k^-	$\Delta f_k(r)$	S_k^+	S_k^-	S_k^+/S_k^-	$\Delta S_k(r)$	ω_k^+	ω_k^-	$\Delta\omega_k(r)$
C1	-0.2167	-0.0748	-0.1418	-0.0685	-0.0237	2.8960	-0.0449	-1.1834	-0.4086	-0.7748
C2	-0.2989	0.1343	-0.4333	-0.0946	0.0425	-2.2255	-0.1370	-1.6328	0.7337	-2.3665
C3	0.1227	0.0671	0.0556	0.0388	0.0212	1.8288	0.0176	0.6701	0.3664	0.3037
C4	0.1812	-0.0556	0.2368	0.0573	-0.0176	-3.2572	0.0749	0.9896	-0.3038	1.2934
C5	0.0607	-0.0323	0.0931	0.0192	-0.0102	-1.8779	0.0294	0.3317	-0.1767	0.5084
C6	0.3410	-0.1554	0.4964	0.1078	-0.0492	-2.1937	0.1570	1.8624	-0.8489	2.7113
C21	0.2757	-0.1444	0.4201	0.0872	-0.0457	-1.9092	0.1329	1.5060	-0.7888	2.2949
C22	-0.1461	0.1391	-0.2852	-0.0462	0.0440	-1.0502	-0.0902	-0.7980	0.7599	-1.5580
C23	-0.0014	-0.0415	0.0400	-0.0005	-0.0131	0.0348	0.0127	-0.0079	-0.2265	0.2186
C24	0.1249	-0.0338	0.1587	0.0395	-0.0107	-3.6997	0.0502	0.6824	-0.1845	0.8669
C26	-0.0535	0.0029	-0.0564	-0.0169	0.0009	-18.560	-0.0178	-0.2924	0.0158	-0.3081
C28	-0.0561	0.1121	-0.1682	-0.0178	0.0355	-0.5007	-0.0532	-0.3066	0.6124	-0.9190
C37	-0.1309	-0.0253	-0.1056	-0.0414	-0.0080	5.1798	-0.0334	-0.7150	-0.1380	-0.5770
C38	0.1622	0.0118	0.1505	0.0513	0.0037	13.783	0.0476	0.8861	0.0643	0.8218
C39	-0.0505	0.0367	-0.0872	-0.0160	0.0116	-1.3758	-0.0276	-0.2757	0.2004	-0.4760
C40	0.0121	0.0228	-0.0107	0.0038	0.0072	0.5323	-0.0034	0.0663	0.1245	-0.0582
C42	0.0185	-0.0010	0.0195	0.0058	-0.0003	-17.974	0.0062	0.1008	-0.0056	0.1064
C44	0.0389	0.0438	-0.0050	0.0123	0.0139	0.8870	-0.0016	0.2122	0.2393	-0.0270

Table 14. The ab initio and DFT calculated the electric dipole moment (Debye), average polarizability ($\alpha_{tot}\times10^{24}$ e.s.u.), and hyperpolarizability ($\beta_{tot}\times10^{-30}$/esu) for compounds **1** and **2**.

Parameters	Compound 1	Compound 2
Dipole moment		
μ_x	2.4590	-3.9437
μ_y	-4.3376	-2.0043
μ_z	-0.3065	-0.3716
μ	4.9955	4.4340
Polarizability		
α_{xx}	38.4646	-28.6233
α_{yy}	-23.1291	25.3421
α_{zz}	-15.3356	3.2812
α_{xy}	0.5775	23.5234
α_{xz}	6.7912	-2.9448
α_{yz}	-0.2194	-1.7860
α_0	-2.7×10^{-28}	-1.6×10^{-28}
α_{tot}	8.2038	8.0586
Hyperpolarizability		
β_{xxx}	373.2941	-764.7209
β_{yyy}	-27.8990	-25.6061
β_{zzz}	-3.0043	-3.0245
β_{xyy}	-1.1266	-0.1180
β_{xxy}	-122.5290	94.7664
β_{xxz}	-54.6925	-42.7077
β_{xzz}	18.6941	50.7200
β_{yzz}	-20.7543	0.5335
β_{yyz}	-1.6932	5.9881
β_{xyz}	5.9700	-10.0915
β_{tot}	430.8171	718.1616
β_0	3.7219	6.2100

3.13. NMR Analysis

In compound **1**, the aromatic proton signals are found in the range of δ 6.54 to 7.92 ppm, which is the aromatic region. The H26 signal is obtained at δ 10.8 ppm due to the nucleus's deshielding by O25, and hydrogen bonding with N29 shifts the signal downfield. ^{13}C NMR shows 19 different signals, representing the presence of different types of protons. C1 and C5 signals are shifted up-field due to the π-conjugation from N11 [57,58].

In compound **2,** the aromatic protons fall in the aromatic region. H31 shows δ 11.0 ppm, which is accounted for by the presence of hydrogen bonding with N34. C13 represents the presence of different types of carbon. C1 and C5 carbon signals are seen in the range δ 126.54-127.38 ppm, which is contrary to comparing the position with compound **1**. This is evident in the nonexistence of conjugation in compound **2** [63,64].

3.14. NLO properties

Polarizability and hyperpolarizability characterize the response of a molecule to an applied electric field. They affect the molecular interactions. The polarizability and hyper-polarizability values of the dyes are shown in Table 14. When comparing the two compounds, the polarizability of compound **1** is more significant than that of its counterpart, and it can act as a better dye than compound **2** [66]. Urea has good non-linear optical properties and is used as a critical parameter for comparative studies (μ = 1.3732 Debye and β = 3.7289×10^{-31} e.s.u.). For compounds **1** and **2**, the first-order hyper-polarizability by the B3LYP/6-311+G(d,p) method is 3.7219 and 6.2100×10^{-30} e.s.u. Among the compounds studied, compound **1** exhibits value similar to that of urea and compound **2** shows twice the value of urea. Therefore, the compounds under study promote good nonlinear properties [67,68].

3.15. Thermodynamic properties

Thermodynamic parameters, such as zero-point vibrational energy (ZPVE) and entropy, are presented in Table 15. The variation in ZPVE is significant. The total energies of compounds **1** and **2** are presented. Of the two compounds, compound **1** shows the minimum total energy of -1083.4568 a.u. [69,70] parameter for comparative studies (μ = 1.3732 Debye and β = 3.7289×10^{-31} e.s.u.).

Table 15. Theoretically computed energies (a.u.), zero-point vibrational energy (kcal/mol), rotational constants (GHz), entropy (calmol^{-1} K^{-1}) and dipole moment (Debye) for compounds **1** and **2**.

Parameters	Compound 1	Compound 2
Total energies (Hartree)	-1083.4568	-1236.1728
Zero-point energy (kcal/mol)	206.7092	230.2788
Rotational constants (GHz)		
A	0.3244	0.5996
B	0.0783	0.0406
C	0.0659	0.0383
Entropy (cal/mol. K)		
Total	155.1820	178.5390
Translational	43.2870	43.6430
Rotational	36.5040	37.0860
Vibrational	75.3910	97.8090
Dipole moment (Debye)	4.9955	4.4393

4. Conclusion

The compound studied, $C_{21}H_{19}N_5O_2$ (**2**), was synthesized according to the procedures described in the literature and characterized by microanalysis, FT-IR, ^{1}H, ^{13}C and UV-visible spectroscopy techniques. It is theoretically compared with its amine derivative $C_{19}H_{17}N_5O$ (**1**). Compounds **1** and **2** were optimized to local minima using the Gaussian 09 package with the DFT/B3LYP method and the 6-311+G(d,p) basis set. Spectroscopic investigations were conducted for compound **2** according to the proposed structure. DFT-based FT-IR spectra and UV-vis absorption agreed with the experimental spectroscopic data of compound **2**. In vertical excitation studies, two transitions were predicted for the test molecules in all solvents, and there was an increase in the solute-solvent interaction as a result of the increase in dielectric constants. In the FMO analysis, the minor energy gap is predicted in compound **2**, at 3.16 eV; for compound **1**, it is 3.58 eV, paving the way for the transition in compound **2**. The stabilization of the optical gap is observed in the solvent effect. The NBO study sheds light on intermolecular charge transfer and intermolecular hydrogen bonding. Among the test molecules, there are more interactions seen in compound **1** than in its counterpart, making it a prominent candidate for NLO studies. The HOMO-LUMO diagram supports the aromatic nature predicted by NICS and HOMA. For the title compounds **1** and **2**, the first-order hyperpolarizability is 3.72×10^{-30} and 6.21×10^{-30} e.s.u. Of the compounds under investigation, compound **2** shows greater hyperpolarizability than urea. Therefore, the compounds under study promote good non-linear properties and have the potential to be explored as candidates for NLO properties. Compound 1 is not synthesized and is used only for theoretical comparisons.

Acknowledgements

We thank the Department of Chemistry, Annamalai University, Chidambaram, for providing the lab and instrumentation facilities.

Disclosure statement

Conflict of interests: The authors declare that they have no conflict of interest.
Ethical approval: All ethical guidelines have been adhered to.
Sample availability: Samples of the compounds are available from the author.

CRediT authorship contribution statement

Conceptualization: Richard Rajkumar Siluvairaj, Thanikachalam Venugopal; Methodology: Richard Rajkumar Siluvairaj, Thanikachalam Venugopal; Software: Richard Rajkumar Siluvairaj, Vallal Perumal Govindasamy; Validation: Richard Rajkumar Siluvairaj, Thanikachalam Venugopal; Formal Analysis: Periyanayagasamy Vanathu Chinnappan; Investigation: Richard Rajkumar Siluvairaj, Thanikachalam Venugopal; Resources: Rajarajan Govindasamy, Vallal Perumal Govindasamy; Data Curation: Richard Rajkumar Siluvairaj, Vallal Perumal Govindasamy; Writing - Original Draft: Thanikachalam Venugopal, Richard Rajkumar Siluvairaj; Writing - Review and Editing: Thanikachalam Venugopal, Rajarajan Govindasamy; Visualization: Vallal Perumal Govindasamy; Supervision: Thanikachalam Venugopal; Project Administration: Thanikachalam Venugopal, Richard Rajkumar Siluvairaj.

ORCID and Email

Richard Rajkumar Siluvairaj
richardrajkumar@gmail.com
https://orcid.org/0000-0002-0064-8603
Vallal Perumal Govindasamy
vallalg99@gmail.com
https://orcid.org/0009-0003-4479-6928
Rajarajan Govindasamy
rajarajang70@gmail.com
https://orcid.org/0000-0002-4186-189X
Periyanayagasamy Vanathu Chinnappan
vpsamychem@gmail.com
https://orcid.org/0009-0000-5370-1263
Thanikachalam Venugopal
profvt.chemau@gmail.com
pvta1998@yahoo.co.in
https://orcid.org/0000-0003-1076-6272

References

[1]. Zubrys, A.; Siebenmann, C. O. Antituberculous isonicotinylhydrazones of low toxicity. *Can. J. Chem.* **1955**, *33*, 11–14.
[2]. Yoshino, J.; Kano, N.; Kawashima, T. Fluorescent azobenzenes and aromatic aldimines featuring an N–B interaction. *Dalton Trans.* **2013**, *42*, 15826–15834.
[3]. Baryshnikova, E. L.; Makhova, N. N. Thermal and base-induced rearrangements of furoxanylketones phenylhydrazones. *Mendeleev Commun.* **2000**, *10*, 190–191.
[4]. Dimmock, J. R.; Vashishtha, S. C.; Stables, J. P. Anticonvulsant properties of various acetylhydrazones, oxamoylhydrazones and semicarbazones derived from aromatic and unsaturated carbonyl compounds. *Eur. J. Med. Chem.* **2000**, *35*, 241–248.
[5]. Rollas, S.; Gulerman, N.; Erdeniz, H. Synthesis and antimicrobial activity of some new hydrazones of 4-fluorobenzoic acid hydrazide and 3-acetyl-2,5-disubstituted-1,3,4-oxadiazolines. *Farmaco* **2002**, *57*, 171–174.
[6]. Maccari, R.; Ottanà, R.; Vigorita, M. G. In vitro advanced antimycobacterial screening of isoniazid-related hydrazones, hydrazides and cyanoboranes: Part 14. *Bioorg. Med. Chem. Lett.* **2005**, *15*, 2509–2513.
[7]. Özdemir, A.; Turan-Zitouni, G.; Kaplancikli, Z. A.; Tunali, Y. Synthesis and biological activities of new hydrazide derivatives. *J. Enzyme Inhib. Med. Chem.* **2009**, *24*, 825–831.
[8]. Ajani, O. O.; Obafemi, C. A.; Nwinyi, O. C.; Akinpelu, D. A. Microwave assisted synthesis and antimicrobial activity of 2-quinoxalinone-3-hydrazone derivatives. *Bioorg. Med. Chem.* **2010**, *18*, 214–221.
[9]. Li, L.; Li, H.; Liu, G.; Pu, S. A colorimetric and fluorescent chemosensor for selective detection of Cu2+ based on a new diarylethene with a benzophenone hydrazone unit. *Luminescence* **2017**, *32*, 1473–1481.
[10]. Biju, S.; Kumar, S. S.; Sadasivan, V. Synthesis, spectral and single crystal X-ray characterization of 5-(2-(2,3-dimethyl-5-oxo-1-phenyl-2,5-dihydro-1H-pyrazol-4-yl)hydrazono)pyrimidine-2,4,6(1H,3H,5H)-trione and its copper(II) complexes. *Polyhedron* **2018**, *144*, 210–218.
[11]. Bernades, C.; Carravetta, M.; Coles, S. J.; van Eck, E. R. H.; Meekes, H.; da Piedade, M. E. M.; Pitak, M. B.; Podmore, M.; de Ruiter, T. A. H.; Söğütoğlu, L.-C.; Steendam, R. R. E.; Threlfall, T. The curious case of acetaldehyde phenylhydrazone: Resolution of a 120 year old puzzle where forms with vastly different melting points have the same structure. *Cryst. Growth Des.* **2019**, *19*, 907–917.

[12]. Sumathi, P.; Enoch, I. V. M. V. Fluorescence Chemosensing of Mg2+ by Phenylhydrazone of a Difluorenylpiperidin-4-one. *Anal. Bioanal. Chem. Res.* **2019**, *6*(2), 311–317.

[13]. Ramesh Babu, R.; Vijayan, N.; Gopalakrishnan, R.; Ramasamy, P. Growth and characterisation of benzaldehyde semicarbazone (BSC) single crystals. *J. Cryst. Growth* **2002**, *240*, 545–548.

[14]. Vogel, A. I.; Furniss, B. S. *Vogel's textbook of practical organic chemistry*; Longman Scientific and Technical, 1989.

[15]. Rauhut, G.; Pulay, P. Transferable scaling factors for density functional derived vibrational force fields. *J. Phys. Chem.* **1995**, *99*, 14572–14572.

[16]. Scott, A. P.; Radom, L. Harmonic vibrational frequencies: An evaluation of Hartree–Fock, Møller–Plesset, quadratic configuration interaction, density functional theory, and semiempirical scale factors. *J. Phys. Chem.* **1996**, *100*, 16502–16513.

[17]. Frisch, M. J.; Trucks, G. W.; Schlegel, H. B.; Scuseria, G. E.; Robb, M. A.; Cheeseman, J. R.; Montgomery, J. A.; Vreven, T.; Kudin, K. N.; Burant, J. C.; Millam, J. M.; Iyengar, S. S.; Tomasi, J.; Barone, V.; Mennucci, B.; Cossi, M.; Scalmani, G.; Rega, N.; Petersson, G. A.; Nakatsuji, H.; Hada, M.; Ehara, M.; Toyota, K.; Fukuda, R.; Hasegawa, J.; Ishida, M.; Nakajima, T.; Honda, Y.; Kitao, O.; Nakai, H.; Klene, M.; Li, X.; Knox, J. E.; Hratchian, H. P.; Cross, J. B.; Adamo, C.; Jaramillo, J.; Gomperts, R.; Stratmann, R. E.; Yazyev, O.; Austin, A. J.; Cammi, R.; Pomelli, C.; Ochterski, J. W.; Ayala, P. Y.; Morokuma, K.; Voth, G. A.; Salvador, P.; Dannenberg, J. J.; Zakrzewski, V. G.; Dapprich, S.; Daniels, A. D.; Strain, M. C.; Farkas, O.; Malick, D. K.; Rabuck, A. D.; Raghavachari, K; Foresman, J. B.; Ortiz, J. V.; Cui, Q.; Baboul, A. G.; Clifford, S.; Cioslowski, J.; Stefanov, B. B.; Liu, G.; Liashenko, A.; Piskorz, P.; Komaromi, I.; Martin, R. L.; Fox, D. J.; Keith, T.; Al-Laham, M. A.; Peng, C. Y.; Nanayakkara, A.; Challacombe, M.; Gill, P. M. W.; Johnson, B.; Chen, W.; Wong, M. W.; Gonzalez, C.; Pople, J. A. Gaussian 03, Revision A.1, Gaussian, Inc., Wallingford CT, 2003.

[18]. Koopmans, T. Über die Zuordnung von Wellenfunktionen und Eigenwerten zu den Einzelnen Elektronen Eines Atoms. *Physica* **1934**, *1*, 104–113.

[19]. Geerlings, P.; De Proft, F.; Langenaeker, W. Conceptual density functional theory. *Chem. Rev.* **2003**, *103*, 1793–1874.

[20]. Pearson, R. G. Recent advances in the concept of hard and soft acids and bases. *J. Chem. Educ.* **1987**, *64*, 561–562.

[21]. Yang, W.; Mortier, W. J. The use of global and local molecular parameters for the analysis of the gas-phase basicity of amines. *J. Am. Chem. Soc.* **1986**, *108*, 5708–5711.

[22]. Mulliken, R. S. Electronic population analysis on LCAO-MO molecular wave functions. III. Effects of hybridization on overlap and gross AO populations. *J. Chem. Phys.* **1955**, *23*, 2338–2342.

[23]. Portella, G.; Poater, J.; Solà, M. Assessment of Clar's aromatic π-sextet rule by means of PDI, NICS and HOMA indicators of local aromaticity. *J. Phys. Org. Chem.* **2005**, *18*, 785–791.

[24]. Chen, Z.; Wannere, C. S.; Corminboeuf, C.; Puchta, R.; Schleyer, P. von R. Nucleus-independent chemical shifts (NICS) as an aromaticity criterion. *Chem. Rev.* **2005**, *105*, 3842–3888.

[25]. Piekarski, A. M.; Mills, N. S.; Yousef, A. Dianion and dication of tetrabenzo[5.7]fulvalene. Greater antiaromaticity than aromaticity in comparable systems. *J. Am. Chem. Soc.* **2008**, *130*, 14883–14890.

[26]. Zborowski, K.; Proniewicz, L. M. Theoretical studies on aromaticity of selected hydroxypyrones and their cations and anions. Part 2. Electron delocalisation in the OCCO group. *J. Phys. Org. Chem.* **2008**, *21*, 207–214.

[27]. Iqbal, P.; Patel, D. S.; Bharatam, P. V. *Ab initio* study on *N,N′,N″*-triaminoguanidine. *J. Phys. Org. Chem.* **2007**, *20*, 1072–1080.

[28]. Jacquemin, D.; André, J.-M.; Perpète, E. A. Geometry, dipole moment, polarizability and first hyperpolarizability of polymethineimine: An assessment of electron correlation contributions. *J. Chem. Phys.* **2004**, *121*, 4389–4396.

[29]. Zeitouny, J.; Aurisicchio, C.; Bonifazi, D.; De Zorzi, R.; Geremia, S.; Bonini, M.; Palma, C.-A.; Samorì, P.; Listorti, A.; Belbakra, A.; Armaroli, N. Photoinduced structural modifications in multicomponent architectures containing azobenzene moieties as photoswitchable cores. *J. Mater. Chem.* **2009**, *19*, 4715–4724.

[30]. Langhals, H. Color Chemistry. Synthesis, Properties and Applications of Organic Dyes and Pigments. 3rd revised edition. By Heinrich Zollinger. *Angew. Chem. Int. Ed Engl.* **2004**, *43*, 5291–5292.

[31]. Datta, A.; Sheu, S.-C.; Liu, P.-H.; Huang, J.-H. Dichlorido*N*′-[(pyridin-2-yl)methylidene-κ*N*]acetohydrazide-κ2*N*′,*O*copper(II). *Acta Crystallogr. Sect. E Struct. Rep. Online* **2011**, *67*, m1852–m1852.

[32]. Qian, H.-F.; Tao, T.; Feng, Y.-N.; Wang, Y.-G.; Huang, W. Crystal structures, solvatochromisms and DFT computations of three disperse azo dyes having the same azobenzene skeleton. *J. Mol. Struct.* **2016**, *1123*, 305–310.

[33]. Kupka, T.; Buczek, A.; Broda, M. A.; Stachów, M.; Tarnowski, P. DFT studies on the structural and vibrational properties of polyenes. *J. Mol. Model.* **2016**, *22*, 101.

[34]. Teimouri, A.; Chermahini, A. N.; Emami, M. Synthesis, characterization, and DFT studies of a novel azo dye derived from racemic or optically active binaphthol. *Tetrahedron* **2008**, *64*, 11776–11782.

[35]. Thomas, K. R. J.; Kapoor, N.; Lee, C.-P.; Ho, K.-C. Organic dyes containing pyrenylamine-based cascade donor systems with different aromatic π linkers for dye-sensitized solar cells: Optical, electrochemical, and device characteristics. *Chem. Asian J.* **2012**, *7*, 738–750.

[36]. Yıldırım, A. Ö.; Yıldırım, M. H.; Kaştaş, Ç. A. Studies on the synthesis, spectroscopic analysis and DFT calculations on (E)-4,6-dichloro-2-[(2-chlorophenylimino)methyl]-3methoxyphenol as a novel Schiff's base. *J. Mol. Struct.* **2016**, *1113*, 1–8.

[37]. Monajjemi, M.; Nouri, A.; Monajemi, H. Qm and ab initio investigation on the hydrogen bonding, nmr chemical shifts and solvent effects on the dppe. *Indones. J. Chem.* **2010**, *7*, 260–272.

[38]. Targema, M.; Obi-Egbedi, N. O.; Adeoye, M. D. Molecular structure and solvent effects on the dipole moments and polarizabilities of some aniline derivatives. *Comput. Theor. Chem.* **2013**, *1012*, 47–53.

[39]. Oyeneyin, O. E.; Adejoro, I. A.; Ogunyemi, B. T.; Esan, O. T. Structural and solvent dependence on the molecular and nonlinear optical properties of 10-octyl thiophene-based phenothiazine and substituted derivatives – a theoretical approach. *J. Taibah Univ. SCI* **2018**, *12*, 483–493.

[40]. Omer, R.; Koparir, P.; Ahmed, L.; Koparir, M. Computational determination the reactivity of salbutamol and propranolol drugs. *Turkish Computational and Theoretical Chemistry* **2020**, *4*, 67–75.

[41]. Sıdır, İ.; Sıdır, Y. G.; Kumalar, M.; Taşal, E. Ab initio Hartree–Fock and density functional theory investigations on the conformational stability, molecular structure and vibrational spectra of 7-acetoxy-6-(2,3-dibromopropyl)-4,8-dimethylcoumarin molecule. *J. Mol. Struct.* **2010**, *964*, 134–151.

[42]. Arivazhagan, M.; Manivel, S.; Jeyavijayan, S.; Meenakshi, R. Vibrational spectroscopic (FTIR and FT-Raman), first-order hyperpolarizablity, HOMO, LUMO, NBO, Mulliken charge analyses of 2-ethylimidazole based on Hartree–Fock and DFT calculations. *Spectrochim. Acta A Mol. Biomol. Spectrosc.* **2015**, *134*, 493–501.

[43]. Demircioğlu, Z.; Kaştaş, Ç. A.; Büyükgüngör, O. Theoretical analysis (NBO, NPA, Mulliken Population Method) and molecular orbital studies (hardness, chemical potential, electrophilicity and Fukui function analysis) of (E)-2-((4-hydroxy-2-methylphenylimino) methyl)-3-methoxyphenol. *J. Mol. Struct.* **2015**, *1091*, 183–195.

[44]. Chocholoušová, J.; Špirko, V.; Hobza, P. First local minimum of the formic acid dimer exhibits simultaneously red-shifted O–H⋯O and improper blue-shifted C–H⋯O hydrogen bonds. *Phys. Chem. Chem. Phys.* **2004**, *6*, 37–41.

[45]. Alabugin, I. V.; Manoharan, M.; Weinhold, F. A. Blue-shifted and red-shifted hydrogen bonds in hypervalent rare-gas FRg–H⋯Y sandwiches. *J. Phys. Chem. A* **2004**, *108*, 4720–4730.

[46]. Alabugin, I. V.; Gilmore, K. M.; Peterson, P. W. Hyperconjugation. *Wiley Interdiscip. Rev. Comput. Mol. Sci.* **2011**, *1*, 109–141.

[47]. Reed, A. E.; Weinstock, R. B.; Weinhold, F. Natural population analysis. *J. Chem. Phys.* **1985**, *83*, 735–746.

[48]. Parr, R. G.; Chattaraj, P. K. Principle of maximum hardness. *J. Am. Chem. Soc.* **1991**, *113*, 1854–1855.

[49]. Sebastian, K. L. On the proof of the principle of maximum hardness. *Chem. Phys. Lett.* **1994**, *231*, 40–42.

[50]. Wang, S.; Cao, J.; Jia, W.; Guo, W.; Yan, S.; Wang, Y.; Zhang, P.; Chen, H.-Y.; Huang, S. Single molecule observation of hard–soft-acid–base (HSAB) interaction in engineered Mycobacterium smegmatisporin A (MspA) nanopores. *Chem. Sci.* **2020**, *11*, 879–887.

[51]. Ashraf, R. S.; Kronemeijer, A. J.; James, D. I.; Sirringhaus, H.; McCulloch, I. A new thiophene substituted isoindigo based copolymer for high performance ambipolar transistors. *Chem. Commun. (Camb.)* **2012**, *48*, 3939–3941.

[52]. Kanimozhi, C.; Yaacobi-Gross, N.; Chou, K. W.; Amassian, A.; Anthopoulos, T. D.; Patil, S. Diketopyrrolopyrrole–diketopyrrolo pyrrole-based conjugated copolymer for high-mobility organic field-effect transistors. *J. Am. Chem. Soc.* **2012**, *134*, 16532–16535.

[53]. Parr, R. G.; Pearson, R. G. Absolute hardness: companion parameter to absolute electronegativity. *J. Am. Chem. Soc.* **1983**, *105*, 7512–7516.

[54]. Gece, G. The use of quantum chemical methods in corrosion inhibitor studies. *Corros. Sci.* **2008**, *50*, 2981–2992.

[55]. Sheela, N. R.; Muthu, S.; Sampathkrishnan, S. Molecular orbital studies (hardness, chemical potential and electrophilicity), vibrational investigation and theoretical NBO analysis of 4-4′-(1H-1,2,4-triazol-1-yl methylene) dibenzonitrile based on abinitio and DFT methods. *Spectrochim. Acta A Mol. Biomol. Spectrosc.* **2014**, *120*, 237–251.

[56]. Ajibade Adejoro, I.; Emmanuel Oyeneyin, O.; Temitope Ogunyemi, B. Computational investigation on substituent and solvent effects on the electronic, geometric and spectroscopic properties of azobenzene and some substituted derivatives. *Int. J. Comput. Theor. Chem.* **2015**, *3*, 50–57.

[57]. Feixas, F.; Matito, E.; Poater, J.; Solà, M. Quantifying aromaticity with electron delocalisation measures. *Chem. Soc. Rev.* **2015**, *44*, 6434–6451.

[58]. Stanger, A. Nucleus-independent chemical shifts (NICS): Distance dependence and revised criteria for aromaticity and antiaromaticity. *J. Org. Chem.* **2006**, *71*, 883–893.

[59]. Ostrowski, S.; Dobrowolski, J. C. What does the HOMA index really measure? *RSC Adv.* **2014**, *4*, 44158–44161.
[60]. Parr, R. G.; Yang, W. Density functional approach to the frontier-electron theory of chemical reactivity. *J. Am. Chem. Soc.* **1984**, *106*, 4049–4050.
[61]. Parr, R. G.; Szentpály, L. v.; Liu, S. Electrophilicity index. *J. Am. Chem. Soc.* **1999**, *121*, 1922–1924.
[62]. Jamróz, M. H. Vibrational Energy Distribution Analysis VEDA 4, Warsaw, 2004-2010.
[63]. Kolandaivel, P.; Praveena, G.; Selvarengan, P. Study of atomic and condensed atomic indices for reactive sites of molecules. *J. Chem. Sci. (Bangalore)* **2005**, *117*, 591–598.
[64]. Okulik, N.; Jubert, A. H. Theoretical analysis of the reactive sites of non-steroidal anti-inflammatory drugs. *Int. Elect, J. Mol. Des.* **2005**, *4*, 17–30. https://biochempress.com/Files/IECMD_2003/IECMD_2003_016.pdf (accessed May 4, 2023).
[65]. Politzer, P.; Concha, M. C.; Murray, J. S. Density functional study of dimers of dimethylnitramine. *Int. J. Quantum Chem.* **2000**, *80*, 184–192.
[66]. Rashid, M. A. M.; Hayati, D.; Kwak, K.; Hong, J. Theoretical investigation of azobenzene-based photochromic dyes for dye-sensitized solar cells. *Nanomaterials (Basel)* **2020**, *10*, 914–937.
[67]. Joshi, B. D. Chemical reactivity, dipole moment and first hyperpolarizability of aristolochic acid I. *J. Inst. Sci. Technol.* **2016**, *21*, 1–9.
[68]. Pathak, S. K.; Srivastava, R.; Sachan, A. K.; Prasad, O.; Sinha, L.; Asiri, A. M.; Karabacak, M. Experimental (FT-IR, FT-Raman, UV and NMR) and quantum chemical studies on molecular structure, spectroscopic analysis, NLO, NBO and reactivity descriptors of 3,5-Difluoroaniline. *Spectrochim. Acta A Mol. Biomol. Spectrosc.* **2015**, *135*, 283–295.
[69]. Obot, I. B.; Johnson, A. S. Ab initio, DFT and TD-DFT electronic absorption spectra investigations on. *Elixir Comp. Chem.* **2012**, *43*, 6658–6661. https://www.elixirpublishers.com/articles/1687775307_201202028.pdf (accessed May 4, 2023).
[70]. Issaoui, N.; Ghalla, H.; Muthu, S.; Flakus, H. T.; Oujia, B. Molecular structure, vibrational spectra, AIM, HOMO–LUMO, NBO, UV, first order hyperpolarizability, analysis of 3-thiophenecarboxylic acid monomer and dimer by Hartree–Fock and density functional theory. *Spectrochim. Acta A Mol. Biomol. Spectrosc.* **2015**, *136*, 1227–1242.